A Thesis
On

Development of a low loss Mn-Zn Ferrite Material for Power Applications

Submitted in the partial fulfillment of requirement for the

Degree in

Master of Technology
IN

Materials Science and Engineering

Submitted by

SAMEER YADAV
6040506

Under the guidance of

Prof. O.P. Pandey and Mr.K. Sriram

School of Physics and Materials Science
THAPAR INSTITUTE OF ENGINEERING AND TECHNOLOGY
(DEEMED UNIVERSITY)
PATIALA (PUNJAB)-147004.
June - 2006

CERTIFICATE

This is to certify that the thesis entitled, **"DEVELOPMENT OF A LOW LOSS MN-ZN FERRITE MATERIAL FOR POWER APPLICATIONS",** submitted by **Mr. Sameer Yadav** in the partial fulfillment of the requirement for the award of the degree of **M. Tech** in **Materials Science and Engineering** from the **School of Physics and Materials Science, Thapar Institute of Engineering and Technology (Deemed University), Patiala,** is a record of candidate's own work carried out by him under our supervision and guidance. The matter embodied in this report has not been submitted in part or full to any other university or institute for the award of any degree.

(Dr. O.P Pandey)

Professor and Head

School Of Physics and Materials Science

Thapar Institute of Engg. &Technology

Patiala, Punjab (147004)

(Mr. K.Sriram)

Manager (R&D)

Cosmo Ferrites Limited

Jabli, Solan

Himachal Pradesh (173209)

Countersigned by:

(Dr. T.P. Singh)

Dean, Academic Affairs

Thapar Institute of Engg. & Technology,

Patiala, Punjab (147004)

Dated:

ACKNOWLEDGEMENTS

I express my deep gratitude and respects to my guides **Dr. O.P Pandey**, **Professor and Head, School of Physics and Materials Science** and **Mr. K. Sriram Manager, R&D, Cosmo Ferrites Limited** for their keen interest and valuable guidance, strong motivation and constant encouragement during the course of the work. I thank them from the bottom of my heart for providing me exposure to the latest Research and Developments in the field of Ferrite Materials. I thank them for their great patience, constructive criticism and myriad useful suggestions apart from invaluable guidance to me.

I am grateful to **Mr. N. S Aiyar, President, Cosmo Ferrites Limited,** for his encouragement, which will forever remain a driving force for me.

I would also like to thank **Dr. Kulvir Singh Assistant Professor and PG Incharge, School of Physics and Materials Science** for his constant guidance and encouragement.

It gives me immense pleasure to express my special thanks to **Mr. Ashish Gautam** and **Mr. Ravinder** who always took keen interest in helping me during my work. I wish my sincere thanks to **Mr. Charanjeet, Mr. Hemraj and Mr. Lekhram** for their cooperation.

I owe my sincere thanks to all the staff members of **School of Physics and Materials Science, TIET, Patiala** and **Cosmo Ferrites Limited**, as well for their support and encouragement.

I would also like to thank my marvelous friends **Ms Komal, Mr. Rajesh,** and **Mr.Chander** for extending their wholehearted support.

Last but not the least; I would like to thank my parents for their moral support that kept my spirit up during the endeavor.

Dedicated To My Parents

CONTENTS **PAGE NUMBER**

CHAPTER 1

INTRODUCTION

Earlier Iron and its alloys were used as magnetic materials to serve the need of the electrical industry for long time. However, with the advent of higher frequencies, the standard techniques of reducing eddy current losses, using lamination or iron powder cores, were no longer efficient or cost effective. This realization stimulated a renewed interest in "magnetic Insulators" as first reported by S. Hilpert in Germany in 1909. It was readily understood that if the high electrical resistivity of oxides could be combined with desired magnetic characteristics, a magnetic material would result that was particularly well suited for high frequency operation.

Research to develop such a material was being done in various laboratories all over the world, such as by V. Kato, T. Takei, and N. Kawai in the 1930's in Japan and by J. Snoek of the Philips' Research Laboratories in the period 1935-45 in the Netherlands. By 1945 Snoek had laid down the basic fundamentals of the physics and technology of practical ferrite materials. In 1948, the Neel theory of ferromagnetic provided the theoretical understanding of this type of magnetic material.

These Ferrites are ceramic, homogeneous materials composed of various oxides with iron oxide as their main constituent. Based upon the chemical composition, soft ferrites can be divided into two major categories, manganese-zinc ferrite and nickel-zinc ferrite. In each of these categories many different MnZn and NiZn material grades are being manufactured by varying the chemical composition or by different manufacturing techniques. The two families of MnZn and NiZn ferrite materials complement each other and allow the use of soft ferrites from audio frequencies to several hundred mega-hertz. The first practical soft ferrite application was in inductors used in LC filters in frequency

division multiplex equipment. The combination of high resistivity and good magnetic properties made these ferrites an excellent core material for these filters operating over the 50-450 kHz frequency range. The large scale introduction of TV in the 1950's was a major opportunity for the fledgling ferrite industry. In TV sets, ferrite cores were the material of choice for the high voltage transformer and the picture tube deflection system. For four decades ferrite components have been used in an ever widening range of applications and in steadily increasing quantities, a few are mentioned in table-1 below.

Table 1 - Soft ferrite applications.

SOFT FERRITE APPLICATIONS	
MAGNETIC DEVICES	**USED IN**
Power transformers and Chokes	High frequency power supplies
Inductors and tuned transformers	Frequency selective circuits
Pulse and wide band transformers	Matching devices
Magnetic deflection structures	TV sets and monitors
Recording heads	Memory storage devices
Rotating transformers	VCR's
Transducers	Vending machines and ultrasonic cleaners

Table 2 - Merits and demerits of ferrites over other magnetic materials.

FERRITES VERSUS OTHER MATERIALS

ADVANTAGES	DISADVANTAGES
High resistivity	Low saturation flux density
Wide range of operating frequencies	Poor thermal conductivity
Low loss combined with high permeability	Low tensile strength
Time and temperature stability	Brittle material
Large material selection	
Versatility of core shapes	
Low cost	

These cubic ferrites are especially useful due to two key characteristics **[1]**:

- High magnetic permeability, which concentrates and enhances the magnetic field.
- High electrical resistivity, which ensures total penetration of the electromagnetic (EM) field.

Furthermore, the dominance of ferrites rests upon a remarkable flexibility in providing tailor-made solutions, ease of preparation, and price and performance considerations. Hence ferrites are widely manufactured into circuit elements, like inductors and cores, reading-writing heads and information storage media.

Amongst the soft ferrites, Manganese Zinc Ferrites are most common, and are used in many more applications than their counterparts, such as nickel-zinc ferrites. Within the Mn-Zn category, large varieties of materials are possible, and the material selection is mainly a function of the application that needs to be accommodated. The application dictates the desirable material characteristics, which in turn determines the chemical composition of the ferrite material. Manganese zinc ferrites are primarily used for frequencies less than 2 MHz. Figure-1 shows the composition diagram for MnZn ferrites in mole% for Ferric oxide, Manganese oxide and Zinc oxide. It identifies the

composition which gives optimum performance for saturation flux density (B_s), low losses (Q) and high initial permeability (μ_i). It also identifies the Curie temperature (T_C) lines for 100 and 250°C. From this composition chart, it is clear that not one composition, of MnZn ferrite, can fulfill all design objectives.

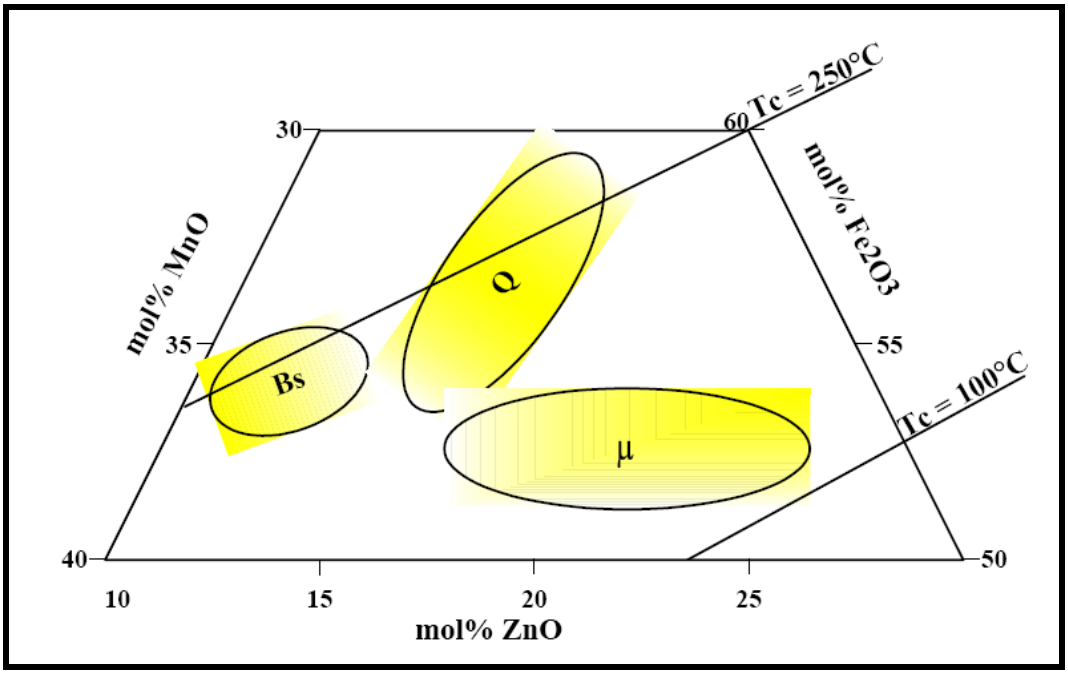

Figure 1 - Composition Diagram for Mn-Zn ferrites.

Nickel Zinc ferrites are characterized by their high material resistivity, several orders of magnitude higher than MnZn ferrites. Because of its high resistivity NiZn ferrite is the material of choice for operating from l-2 MHz to several hundred MHz. To cover such a wide frequency range and different applications, a large number of nickel-zinc materials have been developed over the years. Use of Nickel Zinc ferrites is limited due to their increasing cost. It should be noted that certain nickel chemistries are stress

sensitive and can be adversely changed by some types of stress; this may be a mechanical shock or any grinding operations. Strong magnetic fields from holding devices and fixtures or magnetic chucks used in machining operations may also provide this stress. These resulting changes can include variation in permeability and core loss (lowering of Q). These changes cannot be reversed by degaussing or other electric/magnetic processes.

Manganese Zinc ferrite has the highest permeability and saturation induction of the ferrite class of materials and has the advantage of various stoichiometries with nearly zero magneto-crystalline anisotropy and magneto-restriction, important for stress insensitivity and low noise.

At high frequencies, these soft ferrites have substantial advantages over conventional metallic materials, either in lamination or in powder forming technology. Ferrites offer additional mechanical features as well. Ferrites can be shaped in a variety of different core geometries optimized for specific applications. For example, cores can be designed for ease of assembly, or made self-shielding where required.

Power applications require the transfer of power through the magnetic device, which requires operation of ferrite at high flux density and elevated temperature in the core. Magnetic components of ferrites are used for various applications throughout the industry. The magnetic function of these components in power applications is normally a transformer or inductor.

Main application areas and function for power ferrites are listed as in:

- Automotive Electronics
- Consumer Electronics
- Electronic Data Processing
- Electric Tools
- Household Appliances
- Measurement and control
- Power Conversion
- Telecommunication

With the advent of switched-mode power supplies, the demand for ferrites in power applications has increased significantly. The trend in high frequency power supplies is to go to higher frequencies, which results in size reduction of the magnetic components. This challenge can only be met with soft ferrites.

Desirable ferrite material characteristics for power applications are:

- High saturation flux Density at elevated temperatures (Operating Temperature).
- Low loss at operating frequency, at high flux density and elevated temperature.
- Minimum losses in the operating temperature range.
- High resistivity to minimize the induced eddy currents.

The basic concepts on MnZn ferrites along with the details and current status of low power loss MnZn Ferrites is outlined in literature survey given in Chapter 2. It reveals that MnZn ferrites within a composition range along with other minor substitutions are commonly employed as core material in transformers in power supplies

in automotive electronics, household appliances, power conversion and telecommunication purposes and so on. Chapter 3 describes the experimental work that has been carried out through out the project. This involves the material synthesis, fabrication of sintered ferrite samples, their characterization and evaluation. Results obtained are discussed in Chapter 4. The outcome and conclusion of this work is discussed in Chapter 5 and the scope of future work is outlined in Chapter 6.

In this developmental project, focus is on the synthesis of Mn-Zn ferrite cores of basic composition, 53.23 mole% Fe_2O_3, 35.6 mole% MnO and remaining ZnO, by conventional solid-state reaction route, for power applications, and to study their Electrical and Magnetic properties.

CHAPTER 2

LITERATURE REVIEW

The technology of ferrites or magnetic ceramics has assumed a new importance during the last several decades and especially in the last few years. In addition to the advent of new developments such as radars, satellite communications, memory and computer applications, there has been a corresponding growth in consumer electronics markets in radio, television, power inverters etc. The most recent reason for upsurge in ferrite interest has been the development of the new, small, efficient power supplies using solid state switching, called switch mode power supplies. These power supplies are being used in computers, laptops, microprocessor, telecommunication and entertainment applications.

Requirements for magnetic cores used in switching power supply transformers include soft magnetism, easy magnetization with a small external magnetic field, and low loss. Magnetic materials are classified into two groups, metallic materials and oxide materials. Because the electric resistance of the metallic materials is generally lower, driving the transformer of a switching power supply causes large eddy current loss at high frequencies, typically from several ten hertz to several hundred hertz. In order to suppress loss, oxidic materials, especially MnZn ferrites, are used in the transformer rather than metallic materials [2].

The electromagnetic characteristics of MnZn ferrite are not only dependent on the composition of the main elements but also on the material's microstructure [3]. Because of this, efforts have been made to improve their loss characteristics by controlling the size

of the grains and the distribution of the small amounts of additives in the grain-boundary region [4]. In MnZn ferrites the grain boundaries exhibit different chemical and physical properties than the ferrite grains. The segregation of impurities and the partial re-oxidation of the Fe^{2+} on the grain boundaries during cooling make the MnZn-ferrite grain boundaries highly insulating in comparison to the grain interior. These insulating layers are, in practice, very thin and therefore exhibit a relatively high electrical capacity.

Core loss can be divided into three components: hysteresis loss (P_h), eddy-current loss (P_e) and residual loss (P_r). The proportions of these components in the total loss can vary widely, depending on the measurement conditions such as frequency and magnetic flux density. At low frequencies, hysteresis losses P_h are dominant, and in order to reduce these losses it is important to form a uniform microstructure that is free from lattice defects and pores. At high frequencies, the proportion of eddy current losses P_e increases, but this can be reduced by increasing the resistance of the cores. Eddy-current loss can be decreased by having grain boundaries with a high electrical resistance and by having a ceramic microstructure with small grains. The resistance of the grain boundaries is determined by additives, which are enriched at the grain boundaries during the sintering process, forming an insulating phase. Small grains can be achieved by applying sintering conditions that suppress the grain growth and by choosing additives that act as grain-growth inhibitors. The sintering parameters must lead to a suppression of the grain growth. Therefore, the choice of raw materials, as well as the technological parameters, influences the power losses. In general, two extreme cases regarding the eddy current in

the magnetic core of MnZn ferrites can be identified by applying the brick-wall model [5].

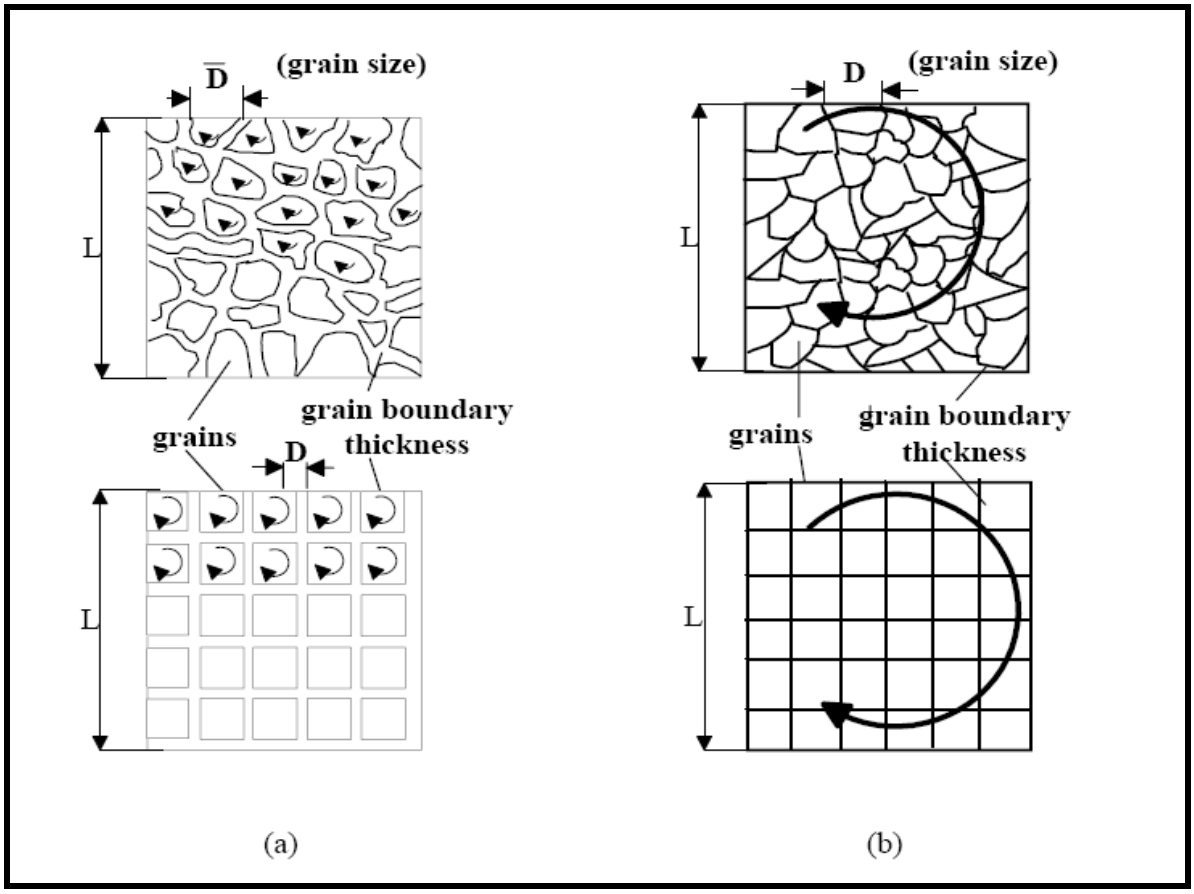

Figure 2 - Brick-wall-microstructure models: (a) schematic picture of a real and an ideal microstructure of a material with isolated magnetic grains exposed to micro-eddy currents. (b) a sketch of an actual and an idealised ferrite microstructure with grain boundaries permeable to the eddy current.[5]

In the first case, when the magnetic grains are isolated and the eddy current in this hypothetical case is localized inside the grains, figure 2(a) the core behaves as an

assembly of individual magnetic grains in which each grain contributes to the eddy-current loss. A different dependence between the total loss and the microstructure holds when the grain boundaries are permeable to the eddy current, figure 2(b). According to this model the bulk material can be approximated by a group of small cubes of size D, separated by high-resistance layers of thickness δ_{gb} and resistance R_{gb}.

Using this model, at low frequencies ($\omega cR << 1$),

$$P_e = cB_m^2 f^2 \cdot \frac{D}{R_{g.b.}^{(mic)}}$$

And at high frequencies ($\omega cR >> 1$), the equivalent relation is

$$P_E \approx \propto \varepsilon_{g.b.} \frac{D}{\delta_{g.b.}}$$

Thus, the eddy-current power loss P_e, which prevails in the frequency range above 500 kHz, can be effectively suppressed by decreasing the average grain size (D), by increasing the grain-boundary resistance and by increasing the grain-boundary width δgb.

According to Barth and Posnak [6], spinel structure, which is the main phase of MnZn ferrite, is composed of Mn, Zn, and Fe ions occupying crystallographic equivalent sites, A and B, with oxygen surrounding these metallic ions, as shown in Figure 3. The magnetic moments assigned to ions at the A and B sites are arranged in parallel in opposite directions by a super-exchange interaction through oxygen. In this configuration, some moments are canceled, which reduces the total magnetic moments compared to that in soft metallic materials, where the magnetic moments are arranged in parallel in the same direction. Therefore, how the constituent elements occupy the A and

B sites determines the total of the magnetic moments. Hence, the magnetic properties such as saturation magnetization, initial permeability etc depends on the super-exchange interactions between ions and therefore is composition dependent.

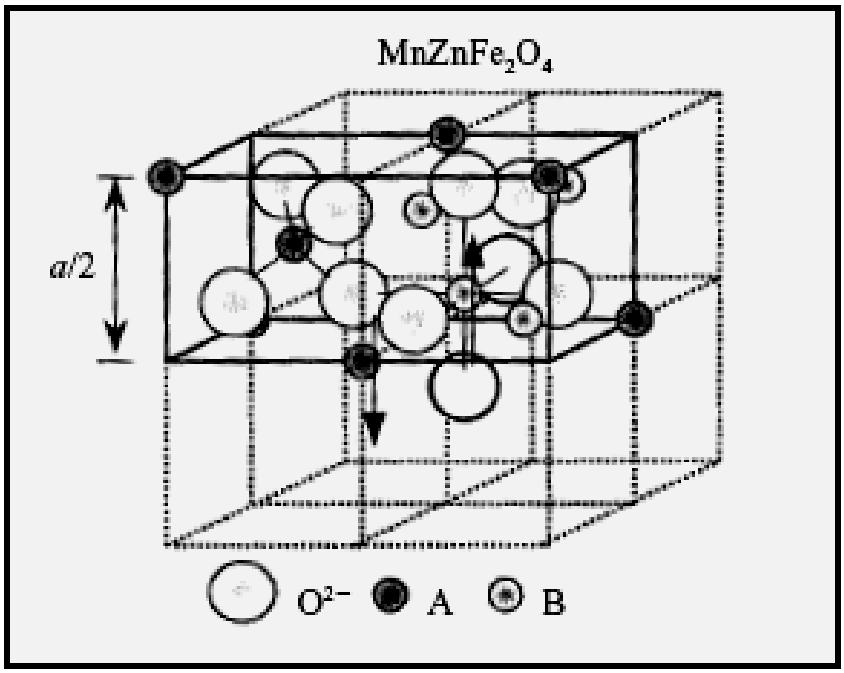

Figure 3- Crystal structure of Ferrite [6]

On the other hand, the requirement of low loss is also related to the main composition. Some ideal compositions exhibit a low magneto-crystalline anisotropy constant and low saturation magneto-striction constant as shown in composition diagram in figure 1.

According to Mitsuo Sugimato [7] outstanding characteristics of low power loss, high saturation and high permeability could be realized only if the following four practices were meticulously followed:

- The accurate estimate of the composition, taking into account magnetic anisotropy or electric resistance;

- The use of ultrapure and ultrafine raw materials;
- The appropriate selection of additives to address the purpose;
- The practice of precise control of the oxygen partial pressure of the sintering atmosphere.

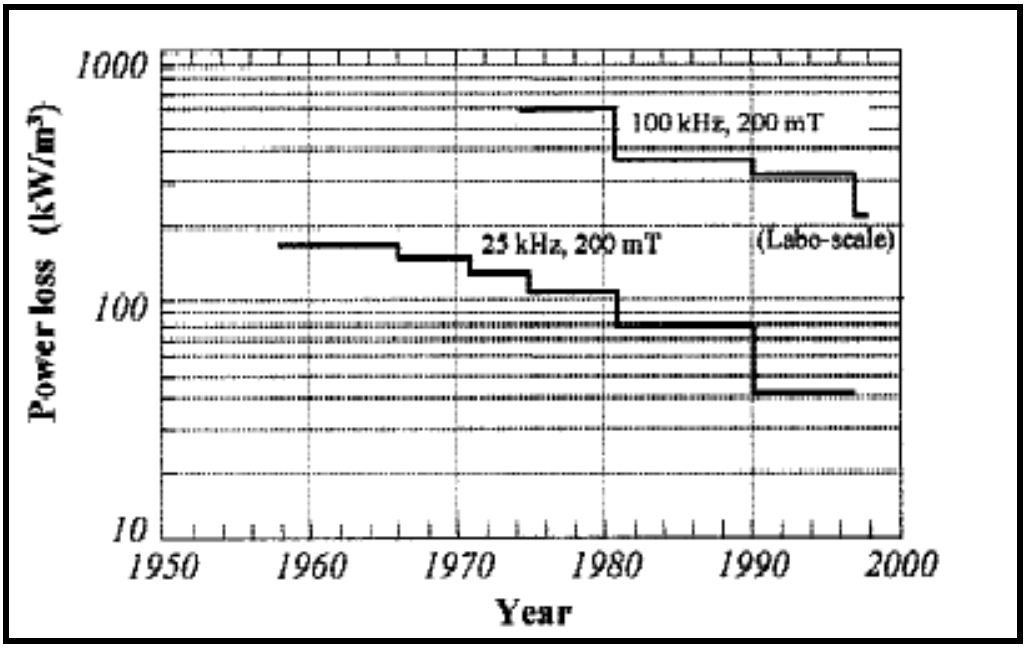

Figure 4 -Improvement in power loss of Mn–Zn ferrite during the second half of the 20th century [7].

According to stoppels [8], miniaturization of electronic devices has lead to the increase in driving frequency to more then 1 MHz and at this high frequency level the power loss dramatically increases, fostering the development of new low-loss materials. The main contributions to the total loss are hysteresis, eddy current and residual losses, respectively, which predominate at different frequencies. A fine-grained homogeneous microstructure with highly resistive grain boundaries is required to minimize eddy

current losses at intermediate and high frequencies. Akashi [9] showed that the simultaneous addition of CaO and SiO_2 to MnZn ferrites made electrical resistivity higher and improved magnetic properties. The additives of CaO and SiO_2 were reported to concentrate around the grain boundaries to form a highly resistive layer. The thickness of the layer was reported to be 1-5 nm and was dependent on the quantity of the additives of CaO and SiO_2, sintering temperature and the heating rate of sintering.

It was further reported by Tsunekawa et al [10] that a large distortion of the spinel lattice near the grain boundaries occurred due to the incorporation of Ca atoms in the spinel lattice and produced deleterious effect on the power loss property of the MnZn Ferrites.

Znidarsic et al [11] reported the effect of Ta_2O_5 in lowering the power loss at high frequencies in MnZn ferrites. Ta_2O_5 was reported to inhibit the grain growth and increased electrical resistivity by segregating at the grain boundaries.

Ishino et al. [12] reported that hysteresis loss as well as eddy current loss decreased by the addition of Ta_2O_5. They regarded the reason for this fact as due to the relatively higher density of the ferrite at the same grain size by the addition of Ta_2O_5.

Hideaki Inaba [13] and his colleagues at Technical Research Laboratories, Kawasaki Steel Corporation, Japan studied the effect of Nb_2O_5 addition in MnZn Ferrites by observing the grain boundary structure and measuring magnetic properties with additives of $CaO\text{-}SiO_2$ and $CaO\text{-}SiO_2\text{-}Nb_2O_5$.They reported that in the samples without Nb_2O_5 addition, Ca and Si atoms concentrate near the grain boundary and are incorporated in the spinel lattice as far as 6 nm, whereas in the samples with Nb_2O_5 addition, Nb atoms concentrated in the grain boundary with a width of 2.5 nm and kept Ca atoms from being incorporated in the spinel lattice by pairing Nb^{5+} and Ca^{2+} ions.

The addition of Nb_2O_5 also promoted the grain growth of MnZn ferrites, which is assumed due to liquid phase sintering that occurred due to the formation of low melting point $(Fe,Mn,Zn)_3O_4\text{-}CaO\text{-}SiO_2\text{-}\ Nb_2O_5$ system.

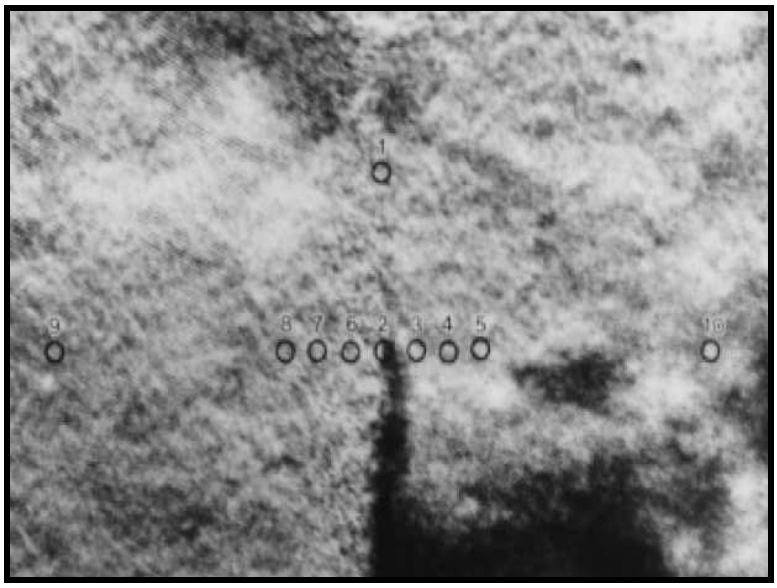

Figure 5 (a)-Lattice image of an Mn–Zn ferrite with Nb_2O_5 addition. A grain boundary is seen in the center of the figure. Circles and numbers indicate the points of EDX analysis shown in Fig below[13].

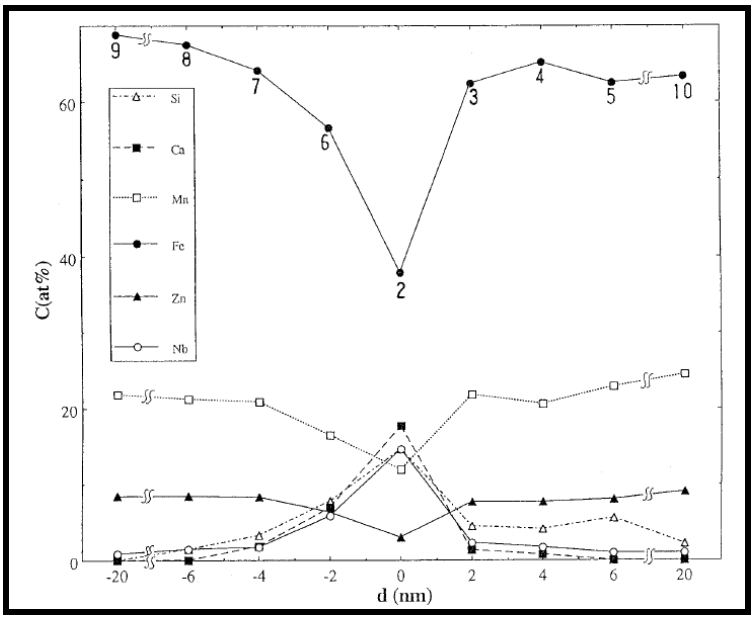

Figure 5 (b) - EDX analysis near the grain boundary shown in 5(a).above. Relative atomic concentrations are shown as a function of the distance from the grain boundary in Nb_2O_5 doped MnZn ferrite sample . Numbers marked in the figure indicate the points shown in figure above [13].

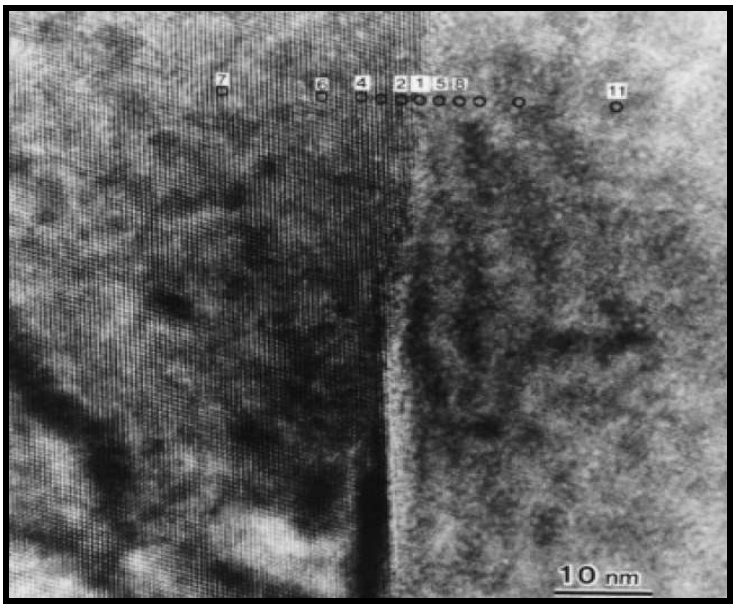

Figure 6(a) - Lattice image of a Mn–Zn ferrite without Nb_2O_5 addition. A grain boundary is seen in the center of the figure. Circles and numbers indicate the points of EDX analysis is shown in Figure below [13].

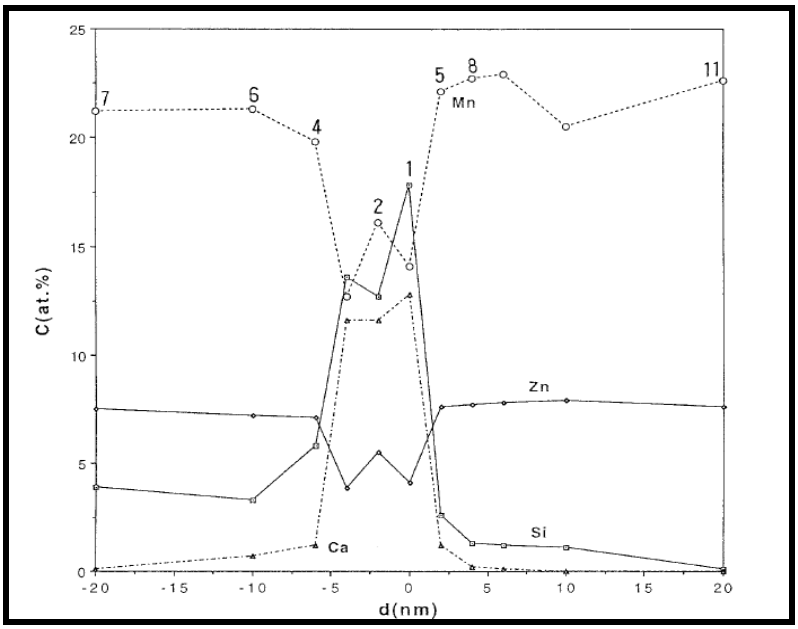

Figure 6(b) - EDX analysis near the grain boundary shown in 6(a). Relative atomic concentrations are shown as a function of the distance from the grain boundary. Numbers marked in the figure indicate the points shown in figure above [13].

Jean-Yves Lavel [14] and his colleagues studied the local electrical behavior, crystallography, and chemistry of grain boundaries in MnZn ferrites. They obtained the reproducible potential images in MnZn ferrites with the voltage contrast method in SEM for the first time. Inter-granular and intra-granular potential drops were compared employing microelectrodes assisted by optical microscopy. They also developed a new method for electrical probing in optical microscopy to provide a direct correlation between the crystallography, chemistry and the potential barriers of grain boundaries. This method clarified the mechanism of eddy current losses in MnZn ferrites to a very local scale and showed that high electrical barriers developed due to strong segregation of Calcium oxide and Silica at the grain boundaries led to high energy GB's, where there are no orientation relationships between adjacent grains; on the other hand, low energy grain boundaries presented orientation relationships and were characterized by low barriers.

In 1999 A. Znidarsic and M. Drofenik [15] investigated the microstructural development and magnetic properties of MnZn ferrites doped with various amounts of CaO and sintered in atmospheres containing various oxygen concentrations. They indicated the strong link among the amount of CaO segregated in the grain boundaries, oxygen concentration during sintering, average grain size and the magnetic properties of the MnZn ferrites. CaO in MnZn ferrites together with low oxygen partial pressure during sintering were recommended for low power loss due to the decreased average grain size, increased grain boundary resistance and high density.

Zaspalis et al. [16] in 2002 worked via grain boundary engineering to modify the magnetic properties of Manganese Zinc ferrites. They investigated the effect of Nb_2O_5 addition on the power loss properties of MnZn ferrites. They proposed that Nb_2O_5, when added in quantities up to 200 PPM, acts as a local grain boundary oxidizing agent that inhibits grain boundary zinc evaporation and therefore helps reducing lattice mismatch and associated residual stresses. The Nb_2O_5 associates with the Ca, creating high electrical resistivity grain boundary phases. They suggested almost 17% improvement of the total power losses that is believed partly due to the reduction of the magnetostriction, stress related hysteresis losses, and partly due to the reduction of the electrical resistivity related eddy current losses.

Chen et al**.** [17] systematically examined the effect of co-doping of V_2O_5 and Nb_2O_5 on the power loss characteristics of MnZn ferrite material. Monotonous increase in the sinter density of the materials was observed with the sintering temperature. Large grain size was observed for samples with large proportion of co-dopants sintered at too high temperature. Samples with large grain size exhibited high power loss and fine grain samples owned small power loss properties and better power loss values.
The prime mechanism responsible for better power loss properties as revealed through complex impedance analysis is the increase in grain boundary resistance.

J. Nie et al. [18] studied the effect of nano-sized silica on the power loss properties of the Mn-Zn ferrites and showed that the magnetic properties of low loss Mn-Zn ferrites are

greatly dependent upon the amount of nano-SiO_2. 50 ppm is the optimum content of the nano-SiO_2 to produce uniform grain structure and lowest magnetic loss. Si atoms are enriched in grain boundaries to prevent Ca and Nb atoms from being incorporated within the spinel lattice, so that a high resistivity layer to lower the power loss can be formed.

Topfer et.al [19] studied the microstructural effect in low power loss ferrites by the addition of various dopants and concluded that the microstructure of the ferrite is determined by a variety of factors such as, raw material quality, calcination temperature, milling procedure and sintering regime. Moreover, the concentration of dopants and impurities effectively regulates the densification process and the grain boundary properties. The effect of CaO and SiO_2 on the microstructure and magnetic properties was studied intensively. SnO_2 and Nb_2O_5 were proposed as an additive, which gets dissolved in the ferrite grains or segregate at grain boundaries and reduce losses. They also correlated the magnetic losses with the sintering temperature and additive concentration.

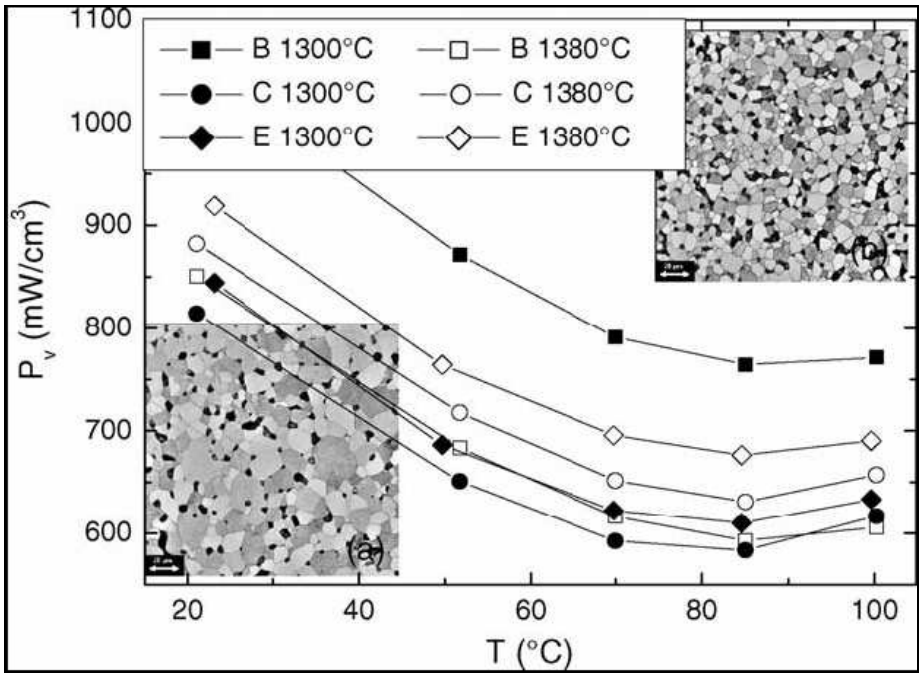

Figure 7 - Power loss at 100 kHz and 200mT as function of temperature for samples with CaO and SiO_2 addition (B) and with SnO_2 (C) and Nb_2O_5 (E).Inset: SEM micrographs of samples B sintered at 1380 ^{o}C (a) and 1300 ^{o}C(b) [19].

Recently Verma et al. [20] developed a new soft ferrite core for power application. They exploited the best properties of both NiZn and MnZn ferrites and developed the Manganese-nickel-zinc ferrite material of $Mn_{0.2}Ni0_{0.3}Zn_{0.5}Fe_2O_4$ composition. The properties of the developed material suited the applications in switch mode power supplies. The power loss of 500 mw/cc was obtained at a frequency of 500 khz and a driving flux density of 50 mT in cores of small dimensions.

Most recently, Ammad H. Qureshi [21] studied the influence of hafnia along with Silica and Calcium oxide on the microstructure and magnetic properties of MnZn ferrites. He

revealed that the substitution of hafnium into MnZn ferrite enhanced the grain growth and 4000 ppm additive level was found to be optimum for the best observed properties.

HfO_2 (wt%)	Power loss (mW/cm^3)			
	No impurities	CaO	SiO_2	CaO/SiO_2
0.2	1340	1214	2261	1078
0.4	1139	1072	2013	878
0.6	1432	1375	2386	1301

Figure 8 - Power loss at 100 mT of samples as a function of additives and impurities.[21]

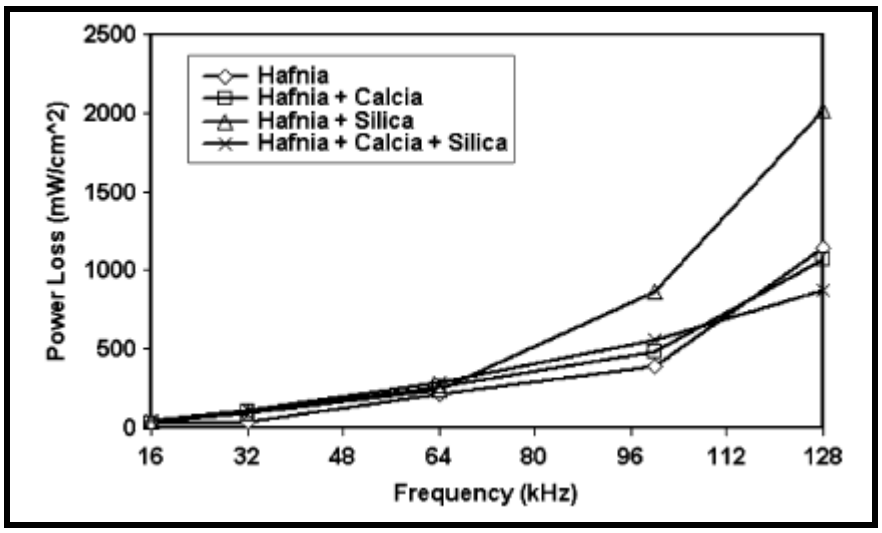

Figure 9- Power loss at 100mT as a function of frequency for 0.4wt% HfO2+SiO2 and CaO [21].

Qureshi concluded that the addition of hafnia along with Silica and calcium oxide produced a balanced microstructure with CaO acting to decrease density and inhibiting grain growth and silica promoting grain growth. Lower power loss was achieved due to higher resistivity induced due to high resistive grain boundaries.

Table 3 - Additives used in MnZn ferrites and their effects on the microstructure.[22].

EFFECT	ELEMENT
Soluble in Spinel lattice	Ti, Co, Cr, Al, Sn, Ni, Cu
Grain growth accelerator	Si, Bi, V, In
Exaggerated grain growth accelerator	B, P, Ba, Sr
Grain growth inhibitor	Ca, Nb, Ta, Zr, Al, Cr
Exaggerated grain growth inhibitor	Mo,W,Na,K

Sezai et al**. [23]** proposed the reduction in core loss in a wide temperature range by dissolving suitable amount of Cobalt oxide in an MnZn ferrite. They found that the stability and reliability of core loss characteristics enhanced under high temperature range by the addition of cobalt. This phenomenon was explained based on magneto crystalline anisotropy K_1, a factor dominating core loss, temperature characteristics of core loss. The core loss becomes minimum at a temperature under which K_1 is close to zero. To reduce the core loss in a wide temperature range, K_1 is made close to zero in a wide temperature range. This compensation of magneto crystalline anisotropy is done by dissolving cobalt ions in the spinel structure of the MnZn ferrite. This could prevent thermal burn-up of an electronic circuit even at high operating temperature.

Historical review of literature gives the idea of increasing the grain boundary resistivity by the addition of Zirconia, which again gets segregated at the grain boundaries along with CaO and SiO_2. It was further confirmed by Stijntjes et al. **[24]** through electron probe microanalysis (EPMA). Other combinations, which gave similar increases in

resistivity and lowered losses, were B_2O_3 + CaO, but this combination is highly susceptible to sintering atmosphere and leads to exaggerated grain growth.

CHAPTER 3

EXPERIMENTAL

This chapter highlights the experimental work carried out in different stages of the project, which involves

- Preparation of Ferrite powder and its characterization.
- Forming powder into cores.
- Firing or Sintering.
- Characterization and testing of cores.

All the steps involved in the ferrite synthesis are given in a nutshell in the flowchart in **figure 10**. Each step is discussed in detail in the following paragraphs.

3.1 Powder Preparation

The ferrite powders were produced by conventional ceramic processing technique, which is one of the most critical steps that control the electrical and magnetic properties of the finally obtained ferrite cores. It consisted of following steps:

3.1.1 Dry Mixing

High purity raw materials of the basic composition 53.23 mole% ferric oxide (99.8% purity), 35.60 mole% manganese oxide (92% purity) and remaining 11.17 mole% zinc oxide (99.4% purity), were mixed and blended homogenously through dry mixing in the pot mill for few hours.

3.1.2 Calcination

Homogenously blend of raw material mixture is further exposed to temperature of 950 ^{o} C for 90 minutes in air atmosphere in the batch type furnace. The purpose of calcining is to start the process of forming of spinel ferrite lattice. This process is essentially one of inter-diffusing phenomenon of substituent oxides into a chemically and crystallographically uniform structure. The driving force for the interdiffusion is the temperature and concentration gradient. As the individual oxides inter-diffuse, some ferrite is created at the interface. This complete phase reduces further diffusion because the concentration gradient is no longer present to act as a driving force. The material in the centre of each oxide particles remains as such, as they experience the difficulty in diffusing through the ferrite since the diffusion distance becomes larger. Since some shrinkage occurs in calcining, one advantage of the process is to reduce the shrinkage in the final sintering. This allows better control of the final dimension of the sintered core. In addition, calcining helps in evaporation of the volatile impurities and homogenization of the powder mixture.

During this process, the powder coarsens considerably, and the colour changes from red to grey or black. The degree of calcining action, or in other words spinel formation can be studied from the X-ray Diffraction (XRD) pattern. It shows the peaks of spinel phase formed and the unreacted residual Fe_2O_3 or hematite phase.

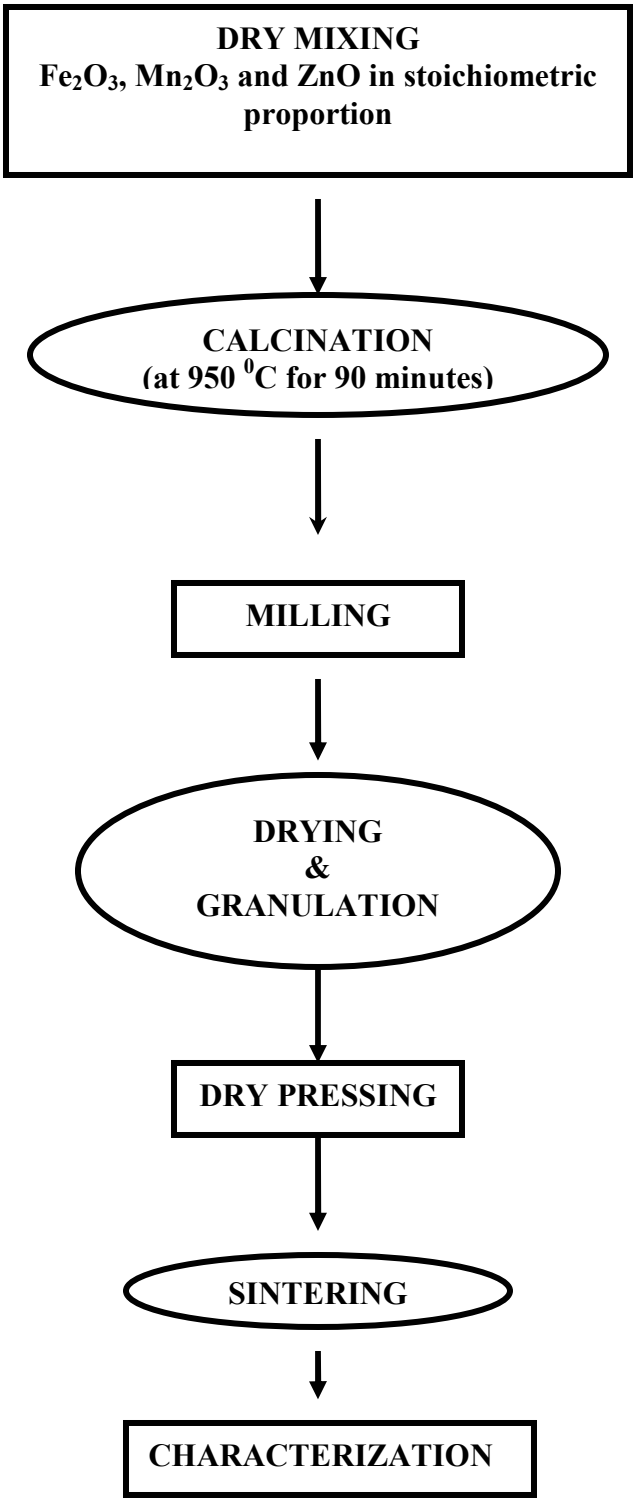

Figure 10 - Flow sheet for the synthesis of sintered Manganese Zinc Ferrites.

3.1.3 Milling

After calcining, the material is broken up by ball milling and attrition action. The particle size reduction is carried out to achieve the desired specific surface area (SSA) of 4200 cm^2/gm through ball milling with 30 mm steel balls followed by fine milling in attritor with 6 mm steel balls. The amount of milling determine the particle size distribution, which in turn influence the homogeneity of the compact going into the final firing as well as the microstructure after the sintering process. In the mid-stage of milling, high purity additives such as Silica, Calcium oxide, Zirconium oxide etc in desired quantity are added to the slurry in the ball mill. SSA is measured through Blains apparatus.

In this project a total of eighteen samples were prepared with the same basic composition of 53.23 mole% ferric oxide, 35.6 mole% manganese oxide and 11.17 mole% zinc oxide but varying amount and type of dopants. The composition, dopants level and types are mentioned in the table-4. Variation in the properties of the finally sintered ferrite cores with the amount and type of dopants were studied.

Table 4 - Composition of the MnZn ferrite samples

Sample No.	CaO (PPM)	SiO_2 (PPM)	ZrO_2 (PPM)	Nb_2O_5 (PPM)	CoO (PPM)
1	500	NIL	NIL	NIL	NIL
2	500	20	NIL	NIL	NIL
3	500	50	NIL	NIL	NIL
4	500	70	NIL	NIL	NIL
5	500	100	NIL	NIL	NIL
6	500	120	NIL	NIL	NIL
7	500	150	NIL	NIL	NIL
8	1000	NIL	NIL	NIL	NIL
9	1000	20	NIL	NIL	NIL
10	1000	50	NIL	NIL	NIL
11	1000	70	NIL	NIL	NIL
12	1000	100	NIL	NIL	NIL
13	500	100	200	200	NIL
14	500	100	200	200	200
15	500	100	200	200	400
16	500	100	200	200	600
17	500	100	200	200	800
18	1000	20	200	200	NIL

3.1.4 Drying and Granulation

Slurry obtained after milling is then dried in the oven, so as to remove the moisture and obtain a press-able powder. Organic additives such as Polyvenyl Acetate (PVA) and. Polyethylene glycol (PEG) are employed to facilitate this step. PVA is added as a binder to provide adequate green strength to the pressed compact [25], so that it can be handled easily in the green stage for further processing, PEG acts as a plasticizer so as to soften the particles [26].The mixture of PVA, PEG and dried slurry is than granulated in the agate mortar, so as to obtain free flowing granulates. The granules are classified by mechanical sieving and the fraction between 200 and 500 μm are subsequently used for pressing.

3.2 Forming

The second step in the ferrite processing technology is the forming of the components. In this step, dry pressing of granulates into the torroid core configuration is carried out. Dry pressing or compacting is done in a mechanical press using a combined action of top and bottom punches in a cavity such that torroids of external diameter of 29.13 to 29.20 mm, internal diameter of 17.38 to 17.45 mm and height of 14.17 to 14.25 mm is obtained.

In this process torroid cores with the green density of 3 to 3.2 gm/mm^3 are obtained.

Figure 11 below shows some of the aspects of die pressing.

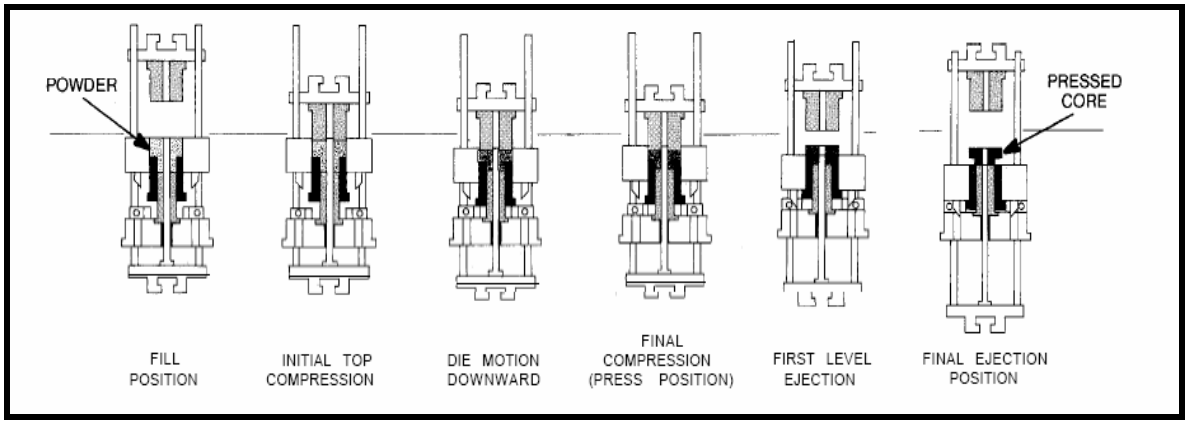

Figure 11- Dry pressing techniques

Before proceeding for dry pressing, granulates are treated with external lubricants such as zinc stearate, which produces a coating of fine lubricant particles on granule surface, as shown in **figure 12** taken from an excerpt from literature**.**

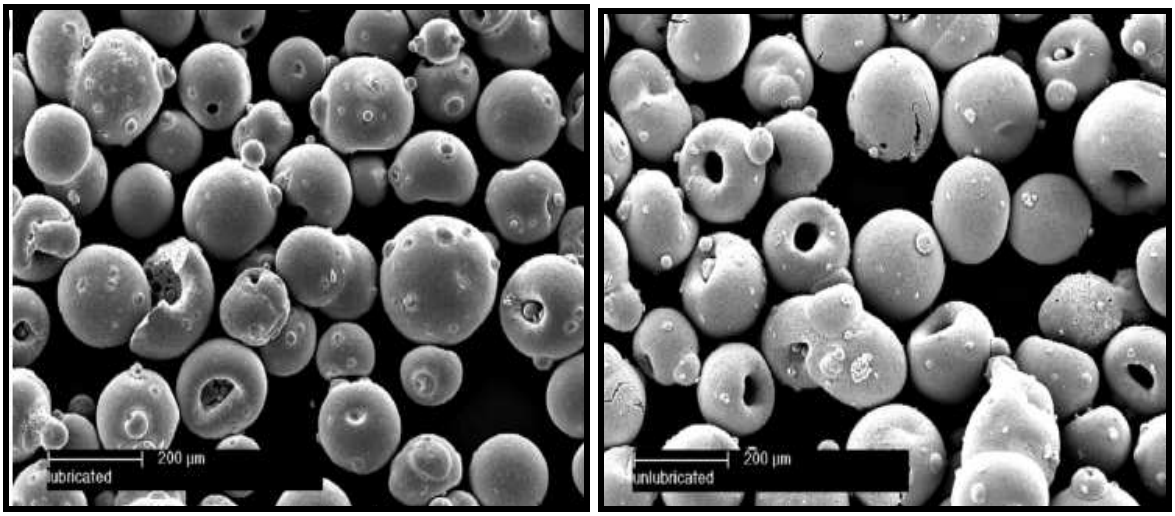

Figure 12- Scanning electron micrographs of granules (a) with external lubricant and (b) without external lubricant. [27]

External lubricants also serve to lubricate the die and punch surfaces. The addition of external lubricant increases tool life [**27**] and helps produce a uniform green body. In addition to providing die-wall lubrication, external lubricants can improve the flow properties of granulated powder by reducing inter-granular friction and hence fill the die more efficiently. Improved packing characteristics can eliminate large inter-granular voids and hence contribute to a low porosity microstructure of the final sintered ferrite core.

3.3 Sintering

This is the most critical step in the ferrite processing. It is during this phase of the process that the product achieves its final electric, magnetic and mechanical characteristics. Sintering of manganese-zinc ferrites requires equilibrium between time, temperature and atmosphere along each step of the sintering cycle. Sintering starts with a gradual ramping up from room temperature to approximately 900 ^{o}C as impurities, residual moisture, binders (PVA, PEG), and lubricants (Zinc stearate) are burned out of the product. The atmosphere in this part of the sintering cycle is 20% oxygen (complete air).

The temperature is further increased to the final sinter temperature of 1360 ^{o}C at high heating rate. While the temperature is increasing, nitrogen gas is introduced into the kiln and the partial pressure of oxygen is maintained at 5% at the sintering temperature of the kiln atmosphere. During the cool-down cycle a reduction of oxygen pressure is very critical in obtaining high quality MnZn ferrites and so the oxygen partial pressure is dropped down to ppm level. Sintering of the green torroid samples is carried out in

programmable Linn batch kiln. Firing schedules and equilibrium oxygen partial pressure conditions maintained are indicated in the sintering profile in the **table 5.**

Figure 13 shows the typical sintering profile carried out in this project

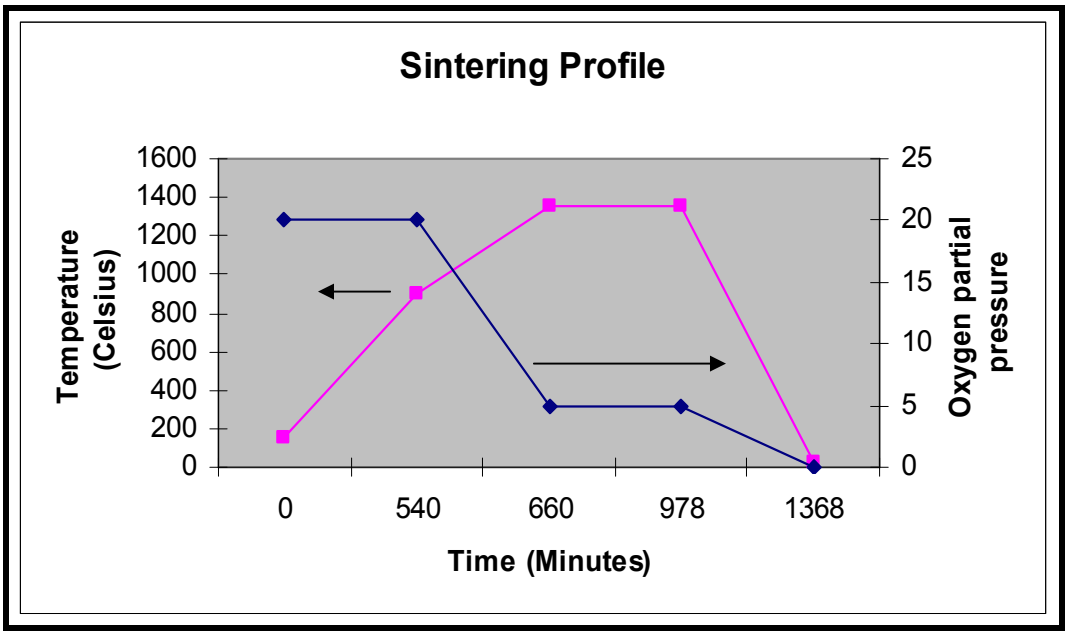

Figure 13- Schematic Diagram of the atmosphere and temperature profiles used during sintering

Table 5- Typical sintering Profile

Sintering Profile			
Time Hrs	**Time(Min)**	**Temp(^{o}C)**	**Oxygen (%)**
0	0	150	20
9	540	900	20
11	660	1360	5
15.3	978	1360	5
22.8	1368	25	0.01

3.4 Characterization

Detailed studies of the Magnetic properties of ferrite samples were carried out. Samples were also put to phase analysis and microstructural characterization.

3.4.1 X-Ray Diffraction (XRD)

XRD analysis of the calcined powder and sintered crush powder is done to study the ferrite phase formation.

3.4.2 Thermo gravimetric Analysis (TGA)

The behavior of the ready to press granulates under increasing temperature was studied through thermo-gravimetric analysis. The analysis was done in the Nitrogen buffer at the temperature of 600 and 1200 ^{o} C at the rate of 10 ^{o}C/min and 20 ^{o}C/min respectively. The weight of the samples was recorded as the function of the increasing temperature. TGA plot gives the clear knowledge about the binder burn out region in the sintering zone.

3.4.3 Electrical and Magnetic Characterization

The measurement of Inductance factor (A_L) and Inductance (L_S) of each sintered torroid was carried out using Hewlett Packard multi-frequency LCR meter (model no.-4275A), and other properties such as initial permeability, were derived using the mathematical relations mentioned in the literature. Inductance Factor A_L (nH), which is the inductance of the coil on the specified core divided by the square of the number of turns, was directly measured through LCR meter under test conditions, of frequency of 10 KHz and voltage

of 150mV, by putting the probes at the centre of each torroid sample. The resistance of the ferrite core was measured by putting the probes of the multi-meter at the two specific points on the ferrite core.

For measuring the Inductance value, the torroid samples were properly wound with the copper wire with 20 turns and the measurements were carried out using LCR meter at the test conditions of frequency set at 10 KHz and voltage of 0.005 Volts.

Initial permeability (μ_i) of the torroid samples with 20 turns in the coil were calculated using the inductance value in the below mentioned mathematical relation [**25].**

$$\mu_I = [4\pi L_S / h \ ln(D_1/D_2)] \quad \text{——} \quad (1)$$

Where h represents the width of the core, D_1 and D_2 are outer and inner diameters of the torroid core respectively.

Variation of initial permeability with temperature was studied using the Curie set up consisting of a wound ferrite sample dipped in the silicon oil containing flask placed over a heater. The ferrite core is uniformly heated at a constant heating rate and the Inductance value corresponding to the temperature is measured by LCR meter. Initial permeability was calculated according to equation (1) and its value is plotted against temperature. Due to the limitations of the available apparatus, Curie temperature of the samples was not measured.

Variation in Initial permeability with frequency is measured similarly through LCR meter and plotted.

Power loss characteristics and magnetic flux density B_{max} of the ferrite samples were studied using power loss analysis set up consisting of Signal generator (Model-FG2002C), Power amplifier (Model no.-EV- 300/F) and Norma AC/DC Power analyzer (Model no.-D5245). Power loss was measured under the conditions of 100 KHz /100 mT and 100 KHz /200mT, Bmax was measured at the frequency 16 KHz, and magnetic field of 250 Amp/m. Variation in power loss and B_{max} with temperature was studied by placing the test samples in the dry heating chamber. Temperature in the heating chamber was varied by the interval of 10 ^{0}C up to 130 ^{0}C and corresponding variation in above mentioned properties was measured.

3.4.4 Microstructural Study

The microstructure of well-ground and polished sintered specimen was studied by optical microscopy using Nikon optical microscope. The samples were etched with Hydrofluoric acid for 2 minutes.

CHAPTER 4

RESULTS AND DISCUSSION

The synthesized ferrite powders and sintered ferrite samples were characterized following the procedure mentioned in Chapter-3**.** Before doing instrumental characterization, powders were visually inspected. Spinel powders were dark grayish/blackish in color. When brought nearer to a permanent magnet, they were strongly attracted to the magnet, suggesting ferrite formation. In this chapter, results obtained from the characterizations are discussed

4.1 Ferrite phase formation (XRD)

The X-ray diffraction pattern of the dry mixed, pre-sintered and sintered crushed core powders are shown in figure-14(a), 14(b) and 14(c). These patterns reveal the sequential phase formation of Manganese Zinc mixed ferrite from dry mixing to final sintering. As revealed by figure 14(c**),** all the peaks in the XRD pattern of sintered crush powder of the synthesized ferrite core are identified and indexed to (Zn Mn Fe) (Fe $Mn)_2O_4$. These patterns reveal the phase formation of Manganese Zinc mixed ferrite.

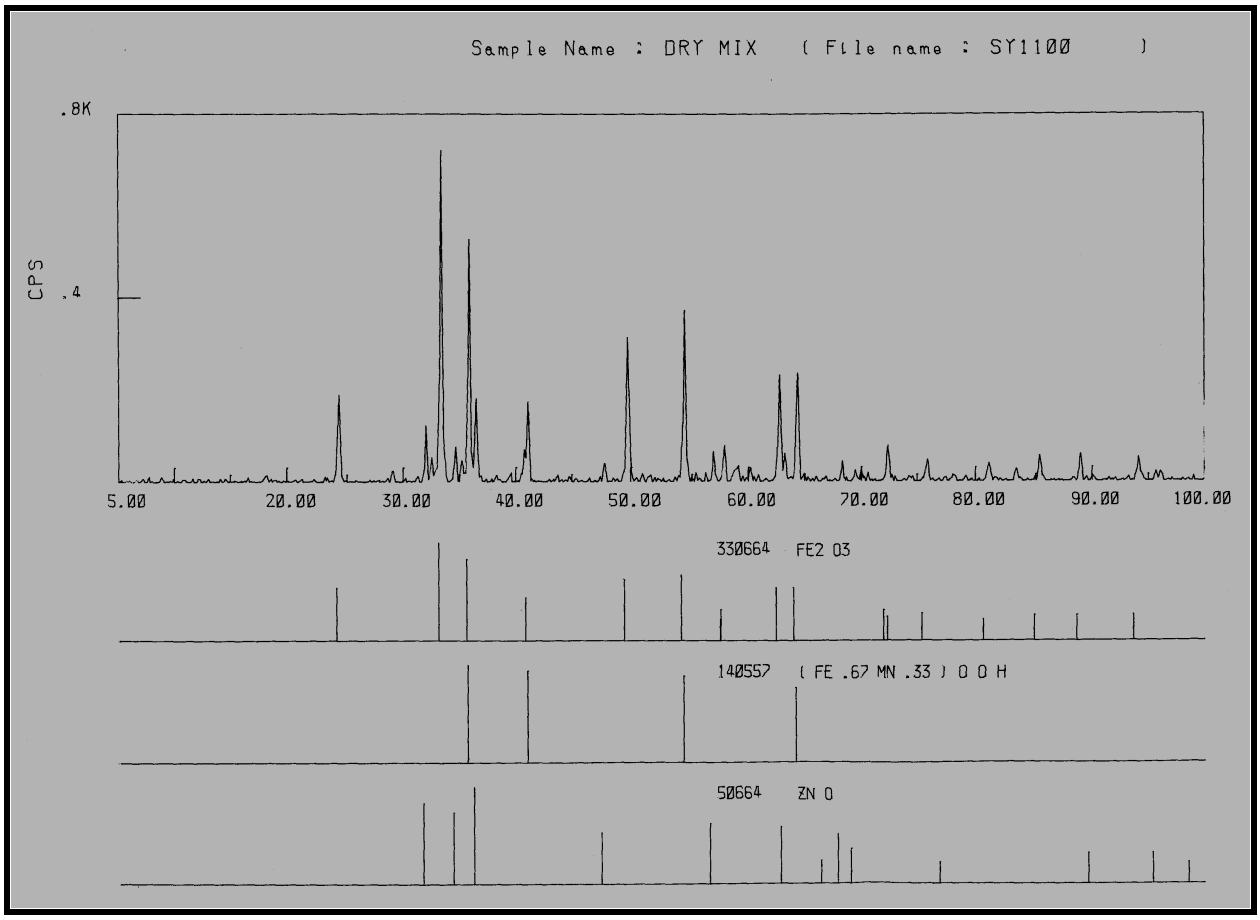

Figure 14(a) - Powder XRD pattern of Dry mixed Powder.

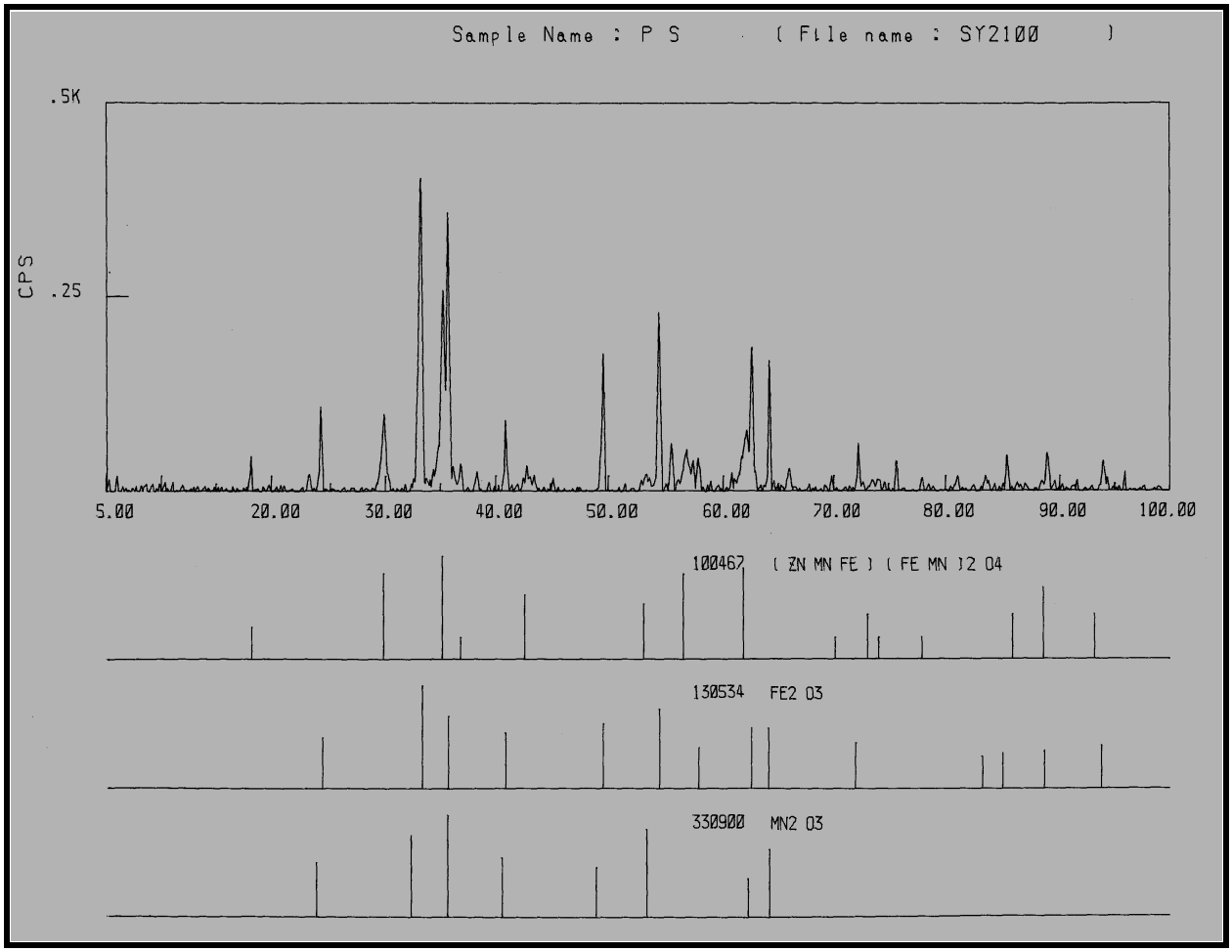

Figure 14(b) - Powder XRD pattern of Pre-sintered Powder.

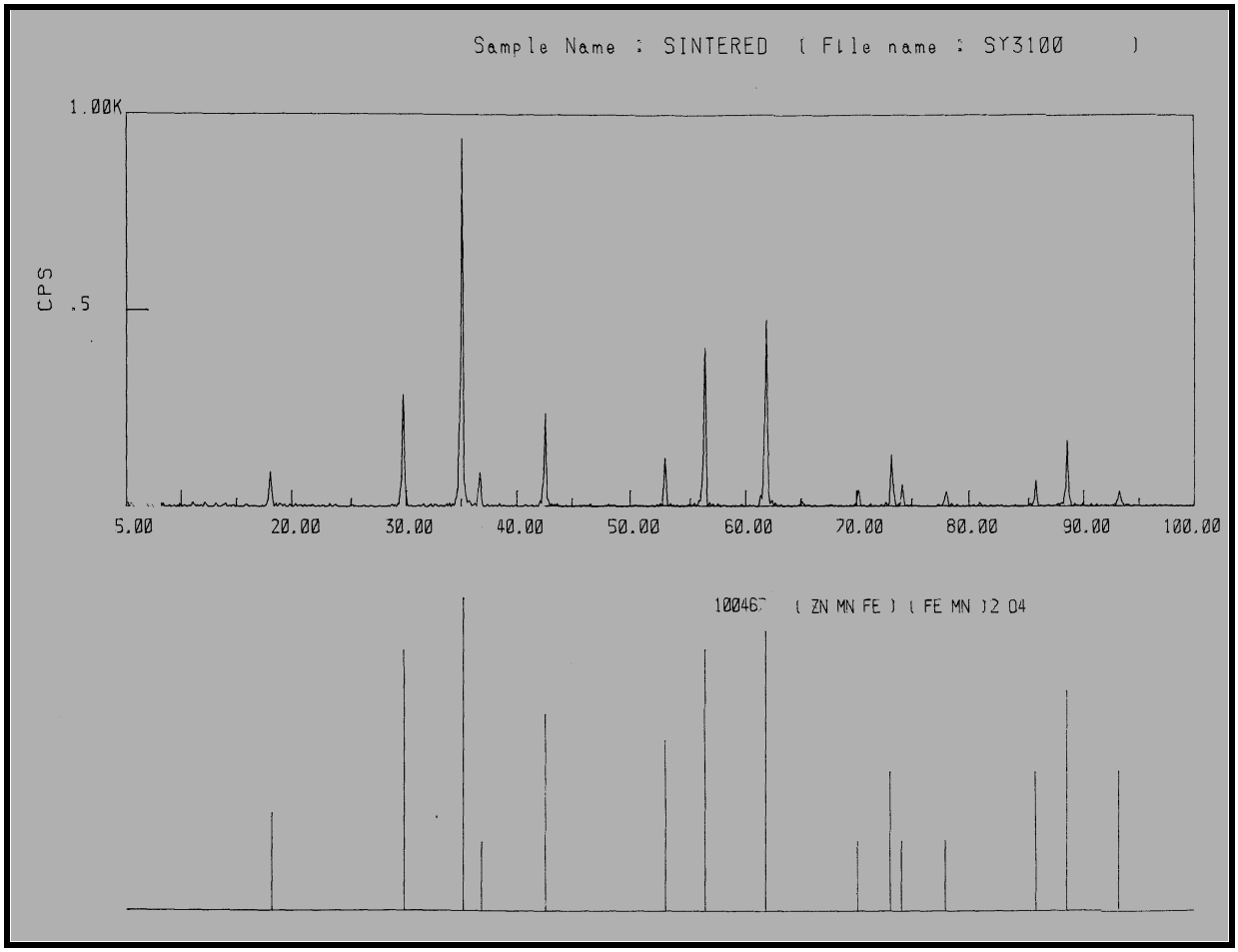

Figure 14(c) - Powder XRD pattern of sintered crushed Powder.

4.2 Thermo-gravimetric Analysis

Thermo gravimetric plots obtained for the ready to press ferrite powder are shown in figure 15. Figure 15(a) shows the binder burn out behavior of the ferrite sample, binder burn out starts at about 150 ^{0}C and drastic loss in mass is observed up to 300 ^{0}C, complete binder burn out seems to occur at 400 ^{o}C.

As known after the initial heating period in which the binder is burned off, the first chemical change occurs in the formation of zinc ferrite starting at 600 ^{0}C and continuing to about 800^{0}C. During this time, Mn assumes its equilibrium form of Mn_2O_3. Shortly after 800^{o}C, MnZn ferrite formation starts slowly with the dissolution of Mn into the Zinc ferrite. Due to higher heating rate, not much information can be extracted from **figure 15(b)**. However, a continuous weight loss in the initial stage is observed.

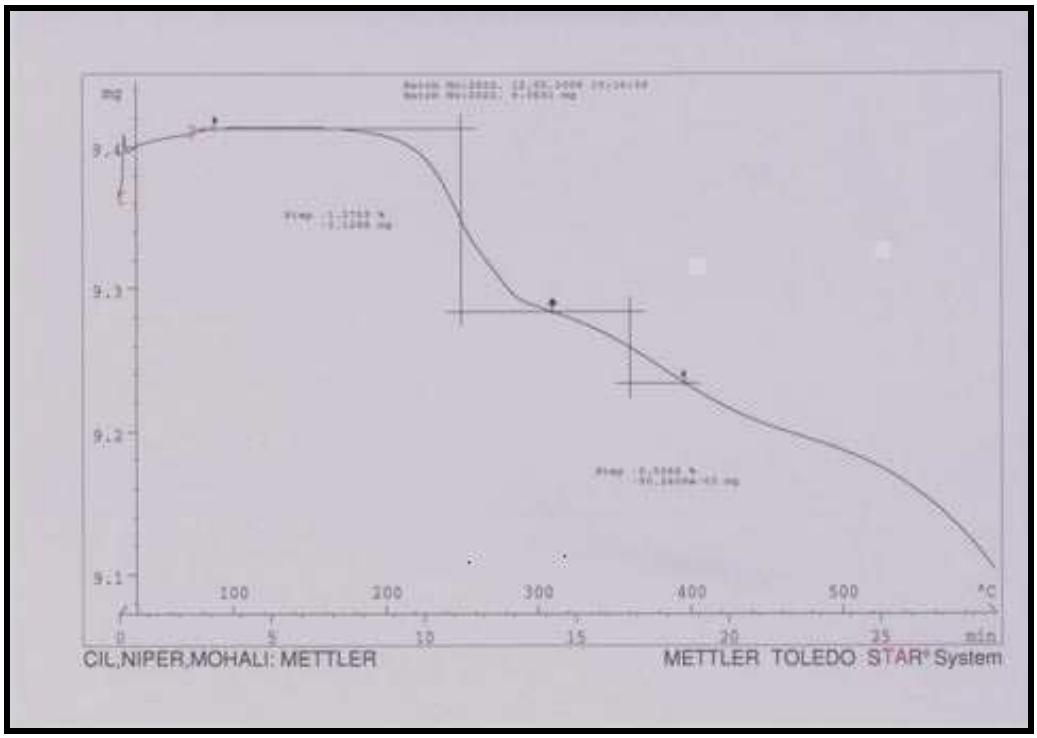

Figure 15(a)- TGA measurements of a MnZn ferrite powder at the heating rate of 10^{o}C/minute

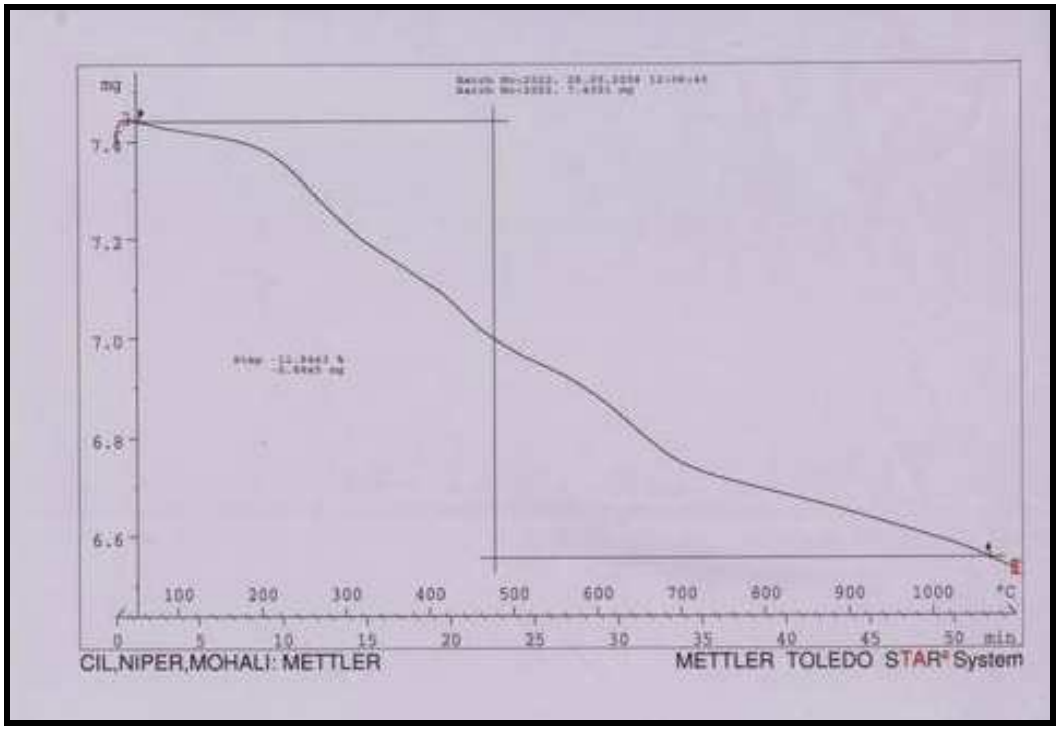

Figure 15(b)- TGA measurements of a MnZn ferrite powder at the heating rate of 20^{0}C/minute.

4.3 Electrical and Magnetic properties

Manganese Zinc ferrite samples synthesized in this work were tested for there electrical and magnetic properties. The outcome of the electrical and magnetic characterization of the samples is discussed in the following paragraphs.

4.3.1 Power Loss Characteristics

Power loss density (P_v) and magnetic flux density (B_{max}) of the ferrite samples were measured through power loss set up as mentioned in the preceding chapter. Power loss was measured under the conditions of 100 khz/100mT and 100 khz/200mT for each sample, Magnetic flux density B_{max} was measured at the frequency of 16 khz and magnetic field strength of 250 A/m. The values of the measured properties are mentioned in **table 6**.

Table 6- Measured values of power loss and magnetic flux density for MnZn ferrite samples.

Sample No.	Power loss [Pv] Kw/m^3 100 khz/100mT		100khz/200mT		Magnetic flux density [Bmax] mT 16 Khz/250 A/m	
	25 C	100 C	25 C	100 C	25 C	100 C
1	156	64	683	403	465	384
2	146	57	653	367	481	401
3	142	52	644	351	469	391
4	137	51	631	338	475	397
5	138	51	624	338	482	401
6	140	53	632	345	478	396
7	144	60	663	383	460	386
8	144	58	663	377	481	398
9	139	51	640	351	484	402
10	141	57	663	384	466	390
11	140	55	644	371	467	388
12	151	66	702	423	453	373
13	128	46	601	328	470	391
14	126	48	582	328	475	394
15	126	50	592	351	469	391
16	115	46	553	328	481	357
17	116	50	556	348	470	392
18	123	43	579	328	475	391

The power loss analysis data of ferrite samples as shown in the **table 6** reveals a substantial variation in power loss with dopants type and amount.

The variation in power loss of the selected samples with variation in silica and calcium content is shown in **table 7** below.

Table 7 - Power loss of MnZn ferrite samples as a function of calcium oxide and silica content

Sample No.	CaO content (PPM)	Silica content (PPM)	Power Loss			
			100khz/100mT		100khz/200mT	
			25 C	100 C	25 C	100 C
1	500	0	156	64	683	403
2	500	20	146	57	653	367
3	500	50	142	52	644	351
4	500	70	137	51	631	338
5	500	100	138	51	624	338
6	500	120	140	53	632	345
7	500	150	144	60	663	383
8	1000	0	144	58	663	377
9	1000	20	139	51	640	351
10	1000	50	141	57	663	384
11	1000	70	140	55	644	371
12	1000	100	151	66	702	423

.

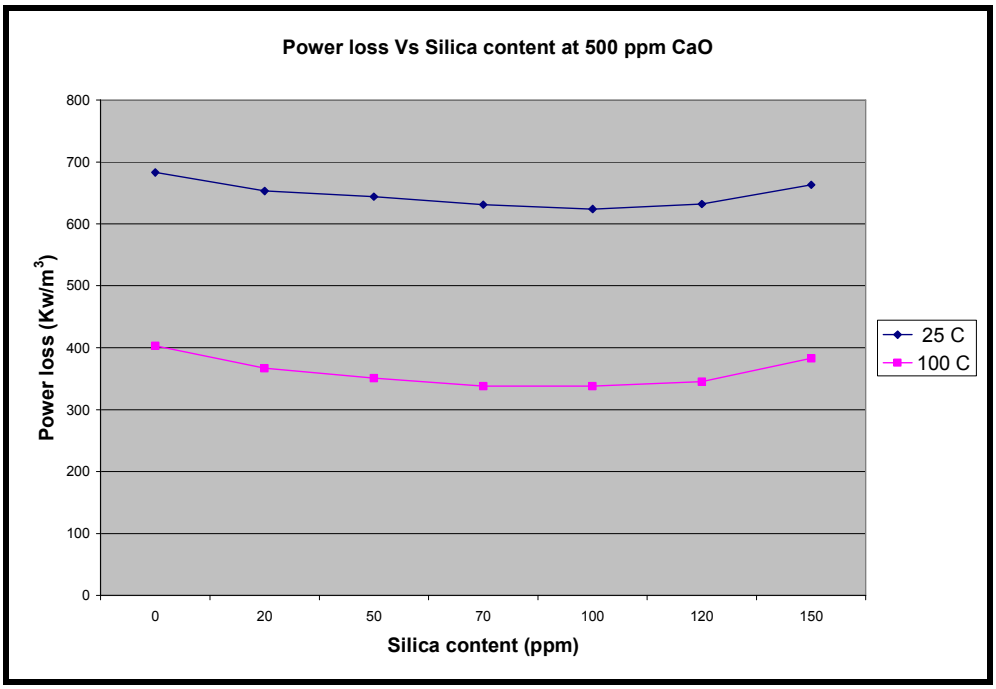

Figure 16 - Variation in Power loss (P_V) at 100 kHz/200mT with silica content for MnZn ferrite samples doped with 500 PPM CaO.

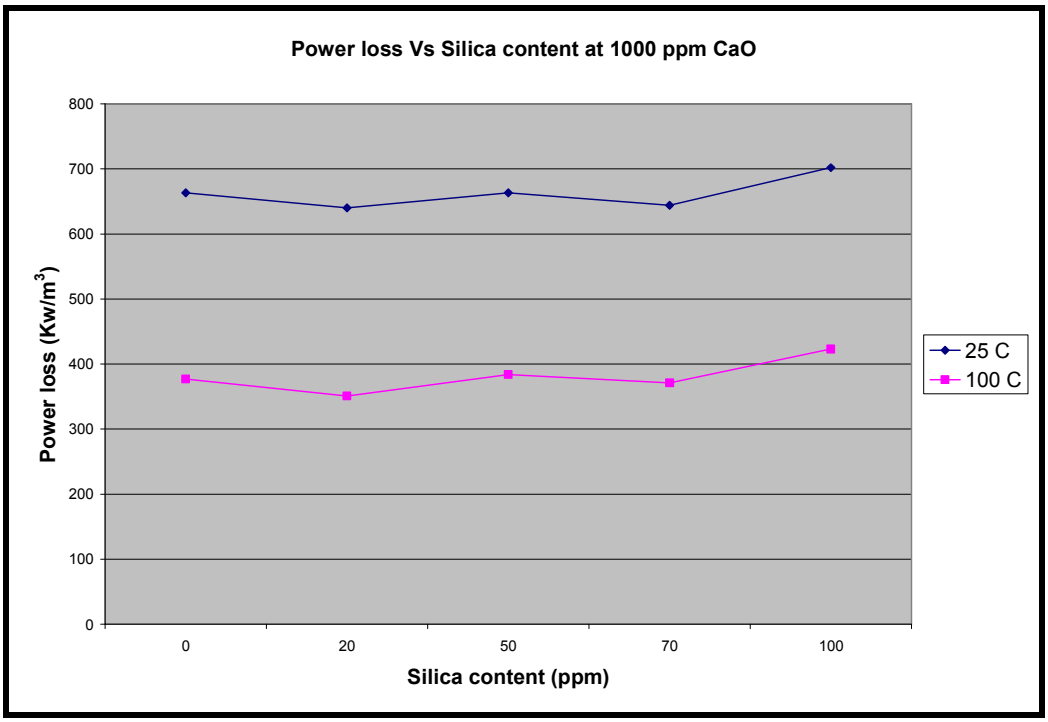

Figure 17 - Variation in Power loss (P_V) at 100 kHz/200mT with silica content for MnZn ferrite samples doped with 1000 PPM CaO.

Figure 16 and 17 shows the variation in total power loss at 100 kHz/200 mT as a function of silica content at a constant level of calcium oxide content for the MnZn ferrite samples. It reveals that the power loss density decreases to a minimum value at an optimum CaO–SiO_2 dopant level and then increases. This optimum amount of CaO-SiO_2 showing lowest power loss is observed to be 500-100 ppm and 1000–20 ppm respectively. The reduction in power loss may be attributed to the formation of highly resistive grain boundaries due to the segregation of CaO and SiO_2 at the grain boundaries [9]. Formation of low melting point insulating phases takes place, which increases the electrical resistivity of the material and consequently the reduction of the eddy currents, developed through the core under alternating currents and finally the reduction in total power loss occurs.

CaO acts as grain growth inhibiter and gets precipitated at the grain boundary and silica is known to promote grain growth, while producing highly resistive grain boundaries. With simultaneous addition of both in optimum amount, leads to the formation of highly balanced microstructure. The addition of SiO_2 above the optimum level causes uncontrollable and inhomogeneous grain growth resulting in high power loss [28]. This exaggerated grain growth annihilates the beneficial influence of CaO and SiO_2 on power loss characteristics and produces the negative effect on the initial magnetic permeability of the ferrite samples.

The best results obtained in terms of power loss with CaO and SiO_2 doping is shown in table 8.

Table 8- Best results obtained by CaO-SiO_2 co-doping in MnZn ferrite samples.

Sample No.	Dopant level (PPM)		Power loss [Pv]			
			100 khz/100mT		100khz/200mT	
	CaO	SiO2	25 C	100 C	25 C	100 C
4	500	70	137	51	631	338
5	500	100	138	51	624	338
9	1000	20	139	51	640	351

As mentioned in above table best power loss properties were observed in the case of sample no. - 4, 5 and 9 at both 100 kHz/100 mT and100 khz/200 mT. Doping level of sample no.-5 (CaO- 500 ppm and SiO_2-100 ppm) and sample no.-9 (1000 ppm CaO and 20 ppm SiO_2) was chosen as an optimum amount for low power loss characteristics and further attempts were made to reduce this power loss to even lower value.

Further reduction in power loss was obtained in sample no.13 and 18 using the optimum levels of CaO and SiO_2 doping as mentioned above, along with 200 ppm of Niobium oxide and 200 ppm of Zirconium oxide. The core losses at low temperature got substantially reduced and the reduction in power loss up to 601/328 kw/m^3 and 579/328 kw/m^3 was observed for the sample no.- 13 with 500 ppm CaO and 100 ppm SiO_2 and sample no.-18 with 1000 ppm CaO and 20 ppm silica at 25/100^o C .

The effect of Zirconia on power loss is yet not clearly mentioned in the literature, but it is known to increase the grain boundary resistivity to a large extent when added along with the traces of Nb_2O_5. It is evident from the measurement of resistance, done by putting the probes of multimeter across the diameter and along the circumference of the torroid samples, that there is a substantial increase in the same with the addition of Nb_2O_5 and ZrO_2. Variation in resistance of the prepared samples is shown in figure 18 .

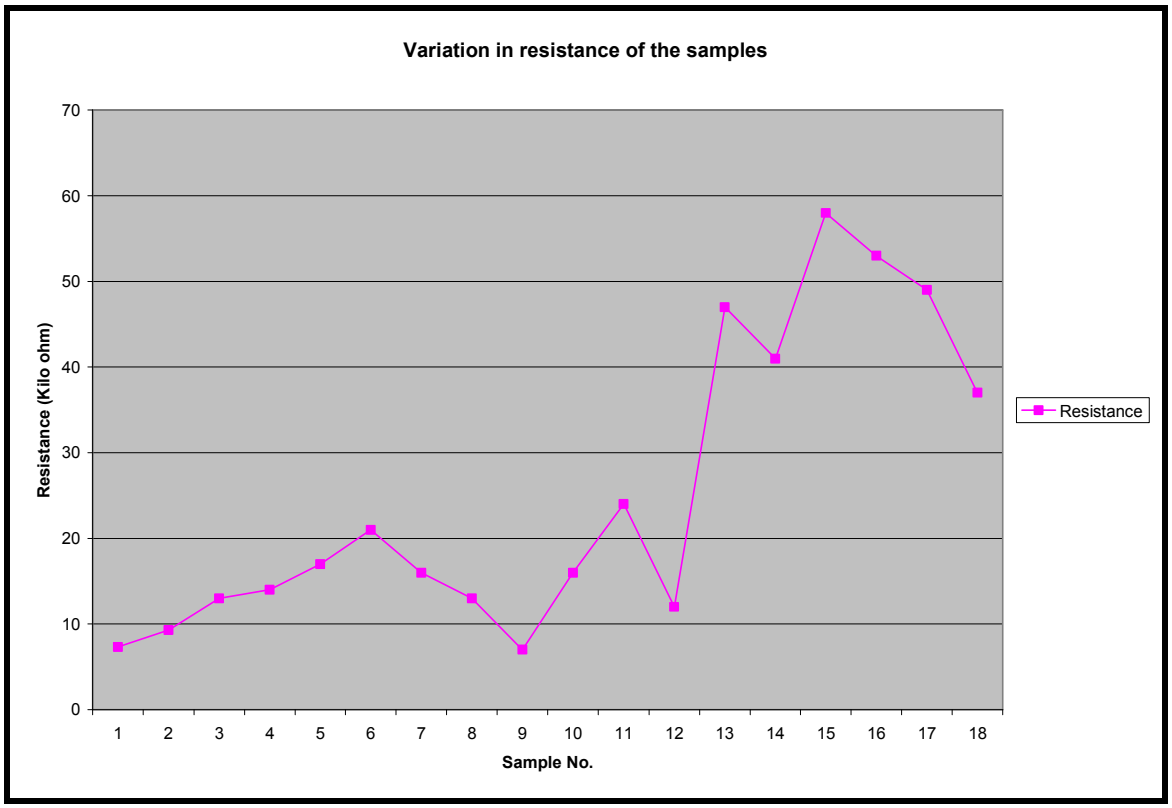

Figure 18- Variation in resistance of the prepared MnZn ferrite samples

The effect of Nb_2O_5 is understood to reduce magnetostriction and stress related hysteresis loss [16] as it acts as a local grain boundary oxidizing agent that inhibits grain boundary Zn evaporation and therefore helps reducing lattice misfit effects and associated residual stresses. Nb atoms gets concentrated at the grain boundaries and keep

calcium atoms from being incorporated into spinel lattice by pairing Nb^{5+} and Ca^{2+} ions preventing lattice distortion.

Sample no. - 14 to 17 were doped with Cobalt oxide in different proportions along with CaO, SiO_2, Nb_2O_5 and ZrO_2. Their power loss properties are shown in table 9.

Table 9- Effect of Cobalt oxide on the power loss properties of the MnZn ferrite samples.

Sample No.	Dopants					Power loss [Pv]			
						100 khz/100mT		100khz/200mT	
	CaO	SiO2	ZrO2	Nb2O5	CoO	25 C	100 C	25 C	100 C
14	500	100	200	200	200	126	48	582	328
15	500	100	200	200	400	126	50	592	351
16	500	100	200	200	600	115	46	553	328
17	500	100	200	200	800	116	50	556	348

As seen in the table 9 above and figure 19, addition of cobalt oxide along with other dopants causes the reduction in the power loss of the MnZn ferrite cores to a greater extent at lower temperature, thus it can be interpreted that it helps in stabilization of power loss in a temperature range.

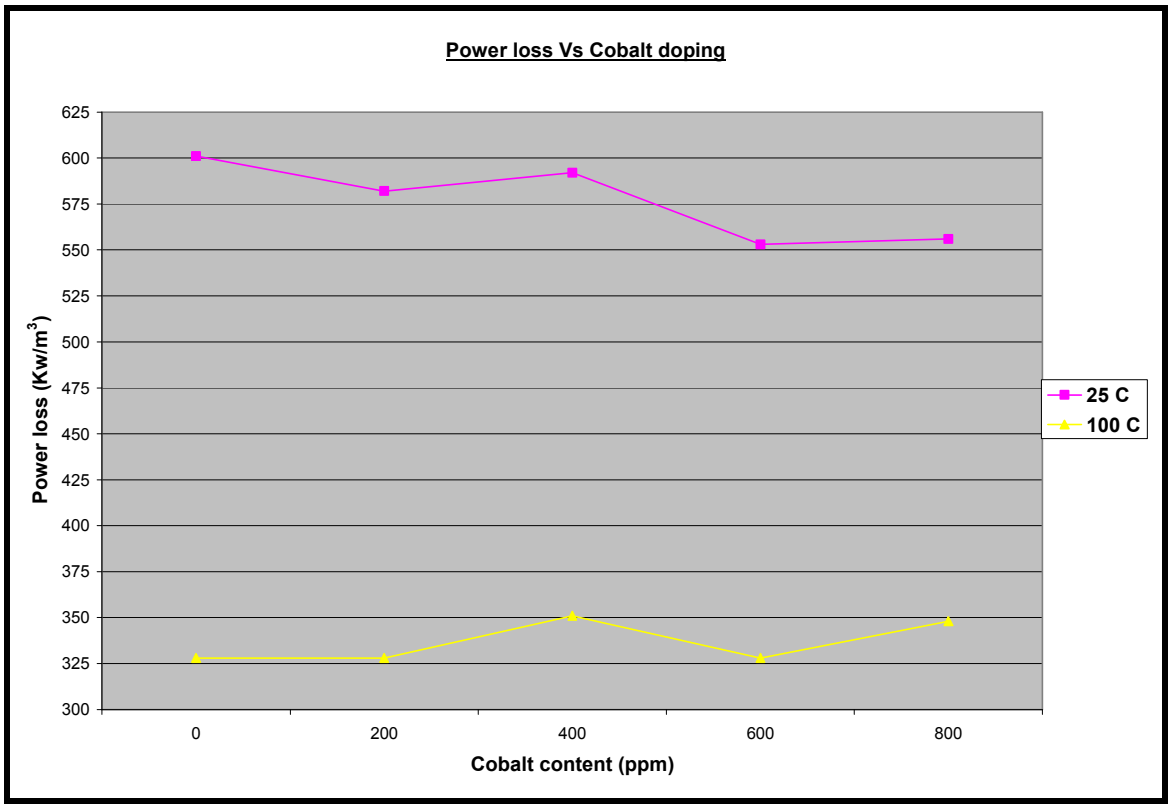

Figure 19 – Variation in power loss at 100 kHz/200 mT with varying cobalt content in MnZn ferrite samples.

Cobalt is known to reduce the core loss in a wide temperature range by dissolving into the spinel structure of MnZn ferrite [23]. Stability and reliability of power loss characteristics is enhanced through cobalt addition by the compensation of magneto crystalline anisotropy. Highest electrical resistance is observed for samples with cobalt doping as evident from figure 18.

Lowest power loss at both 25^{o} C and 100^{o} C is obtained with cobalt doping. Most optimum amount of CoO doping for this composition comes out to be 600 ppm with power loss of 46 Kw/m^3 and 328 Kw/m^3 at 100 khz/100 mT/100^{0}C and 100khz/200mT/100^{0} C respectively. As evident from figure 19, increase in the cobalt

level above 600 ppm increases the power loss slightly at 25^0C but substantially at 100^0C. Hence we may assume that the some temperature stability of power loss is achieved but on the cost of increase in power loss. Variation in power loss with temperature for few selected samples at 100khz/100mT and 100khz/200mT is shown in the figure 20 and 21 below, It clearly shows a substantial power loss drop from sample 1 to sample 18 and also temperature stability is induced in the samples with cobalt oxide doping. This temperature stability is to higher extent at 100 kHz/200mT as evident from the flatness of the curve in the figure.

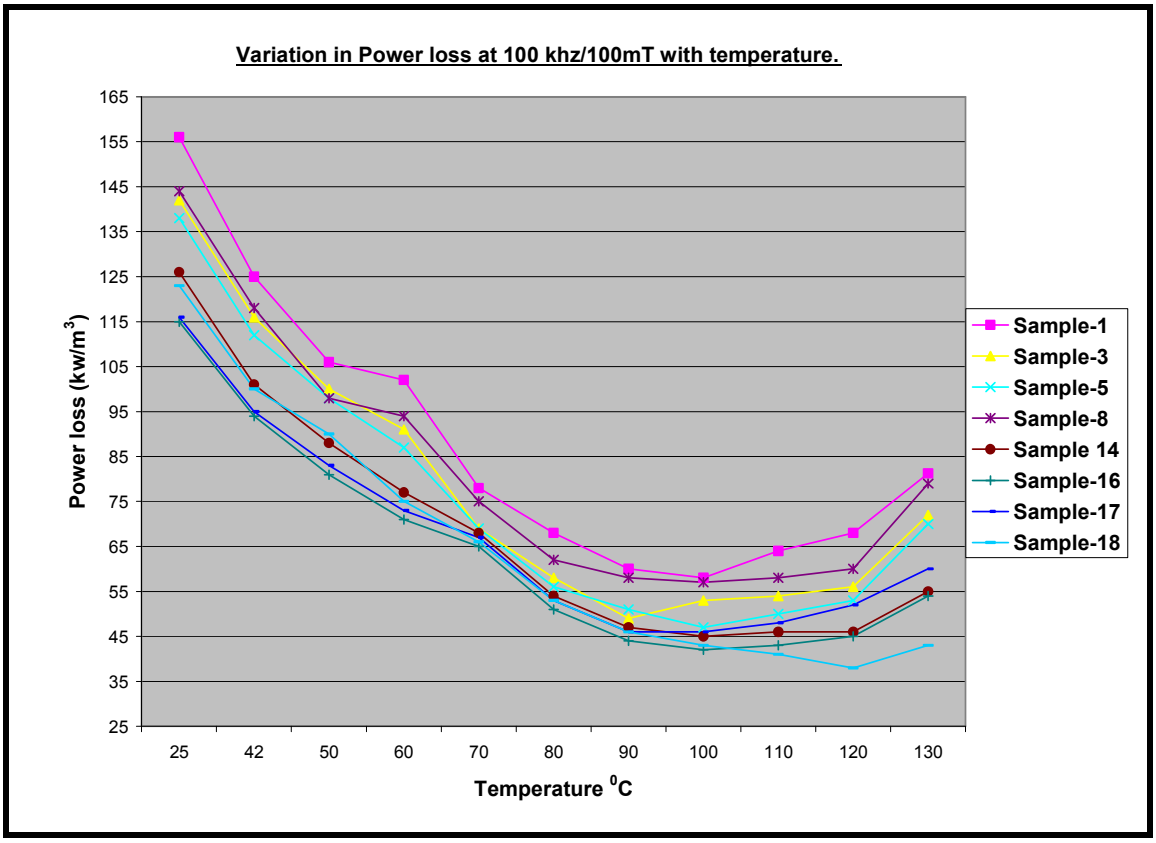

Figure 20- Variation in power loss of MnZn ferrite samples with temperature at 100 khz/100mT.

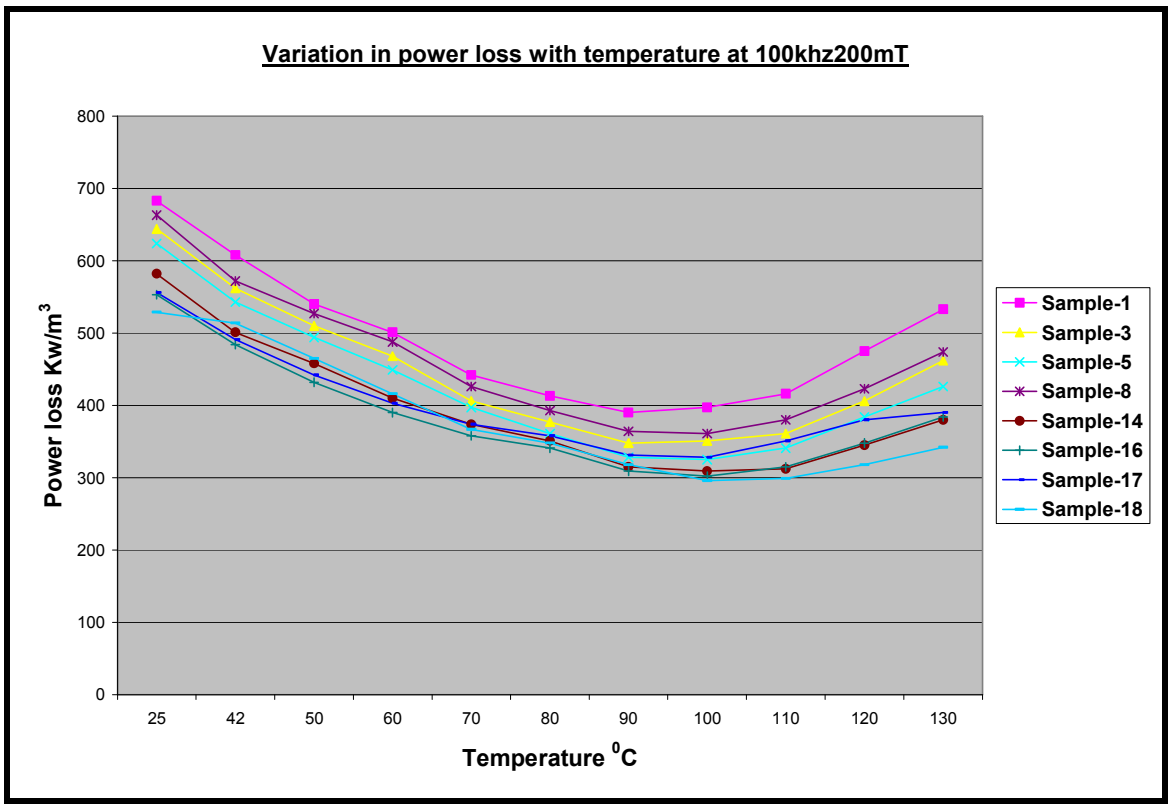

Figure 21 - Variation in power loss of MnZn ferrite samples with temperature at 100 khz/200mT

The minimum power loss point of the ferrite samples with Cobalt doping is obtained to be around 100^0C.

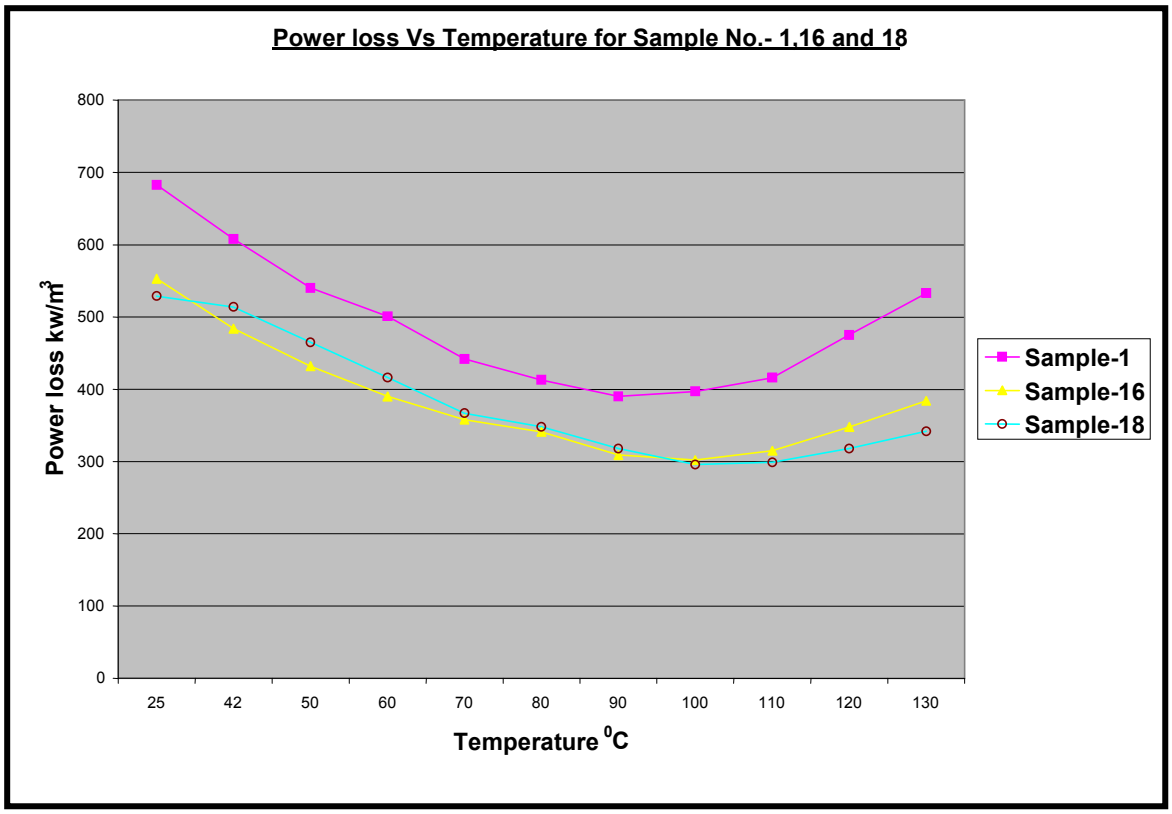

Figure 22- Comparative chart of variation in power loss with temperature for samples no- 1,16 and 18 at 100khz/200mT.

The best results of power loss as well as temperature stability are obtained for sample no. 16 and 18 as revealed by the figure 22 above.

4.3.2 Magnetic flux density

Variation in Magnetic flux density of the samples with temperature measured under the conditions of 16 Khz frequency and applied magnetic field of 250 A/m is plotted in the figure 23 below. A slight increase, though random, is observed in the samples with cobalt doping, overall best magnetic properties seems to be achieved in sample no.- 16 and 17.

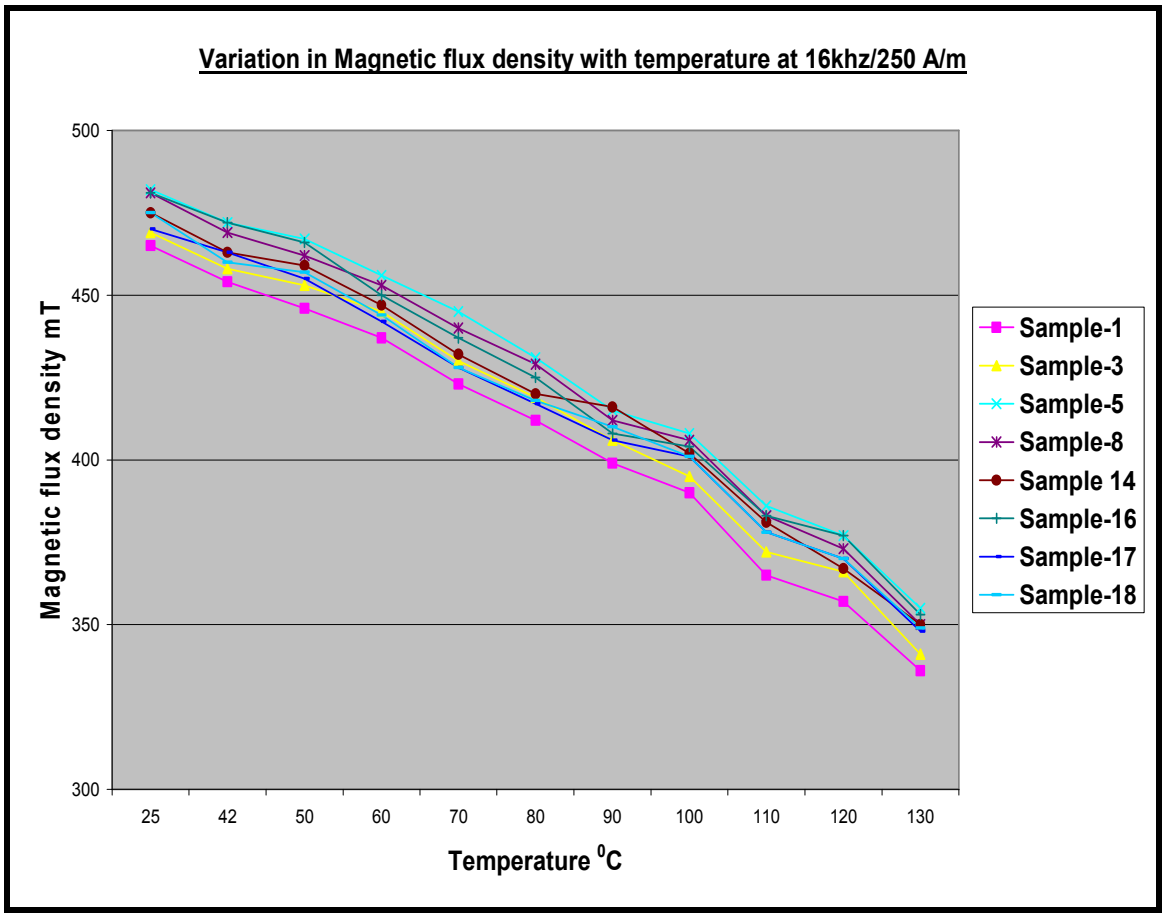

Figure 23- Comparative chart of variation of magnetic flux density (B_{max}) with temperature for synthesized MnZn ferrite samples.

4,3.3 Inductance factor, Inductance value and Initial Magnetic Permeability

Inductance factor (A_L), Inductance value (L_S) and Initial permeability of the MnZn ferrite samples prepared in this work measured under the specific conditions discussed in the previous chapters are mentioned in **table 10.**

Table 10- Inductance value and Initial permeability of the samples

Sample No.	A_L (nH)	Ls (uH)	μ_i
1	2634	1054	2128
2	2762	1105	2186
3	2651	1060	2131
4	2594	1038	2096
5	2544	1018	1998
6	2532	1013	2033
7	2581	1032	1998
8	2673	1069	2121
9	2670	1068	2106
10	2483	993	2001
11	2406	962	1932
12	2328	931	1822
13	2398	959	1901
14	2476	990	1949
15	2414	966	1903
16	2516	1006	1998
17	2483	993	2005
18	2428	971	1911

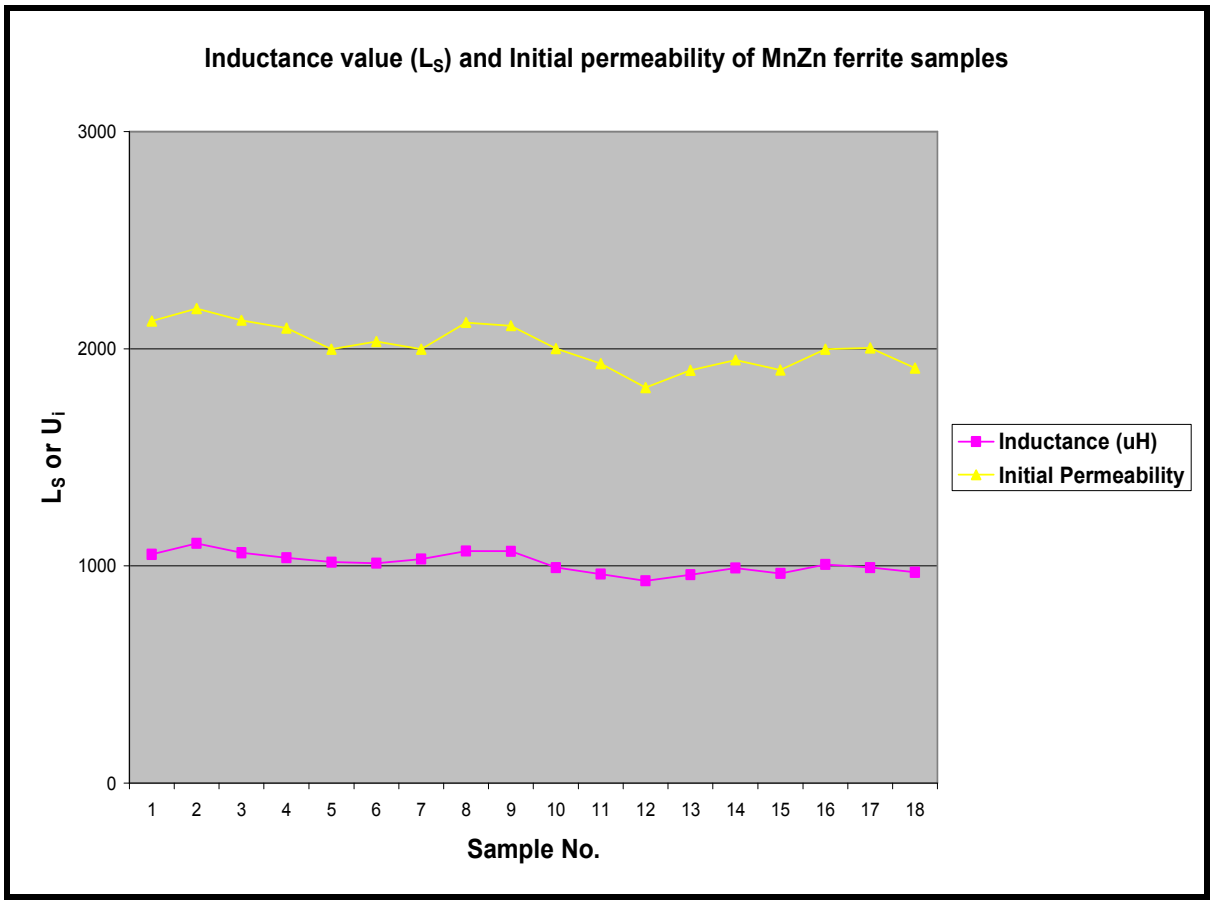

Figure 24- Variation in Inductance value and initial permeability of the ferrite samples

As revealed by the **figure 24** above, slight but not so significant variation is observed in initial permeability and inductance value of the prepared MnZn ferrite samples.

The variation in permeability with frequency and temperature is plotted in **figure 25** and **figure 26** respectively**.** As revealed by the **figure 25**, the operating frequency of the

MnZn ferrite cores of all tested samples is upto 400 Khz without much variation in the initial permeability of the material.

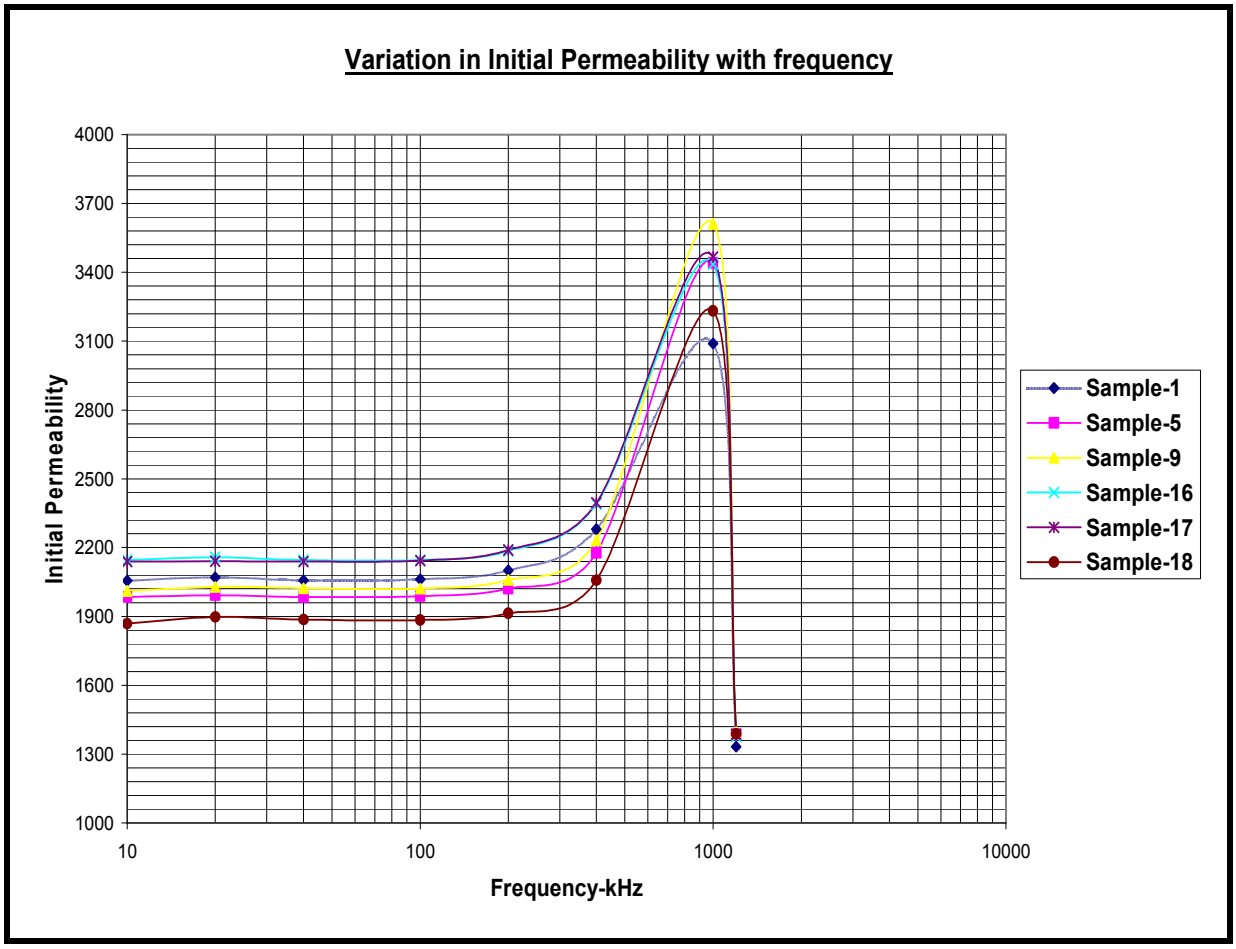

Figure 25 - Variation initial permeability with frequency of the ferrite samples.

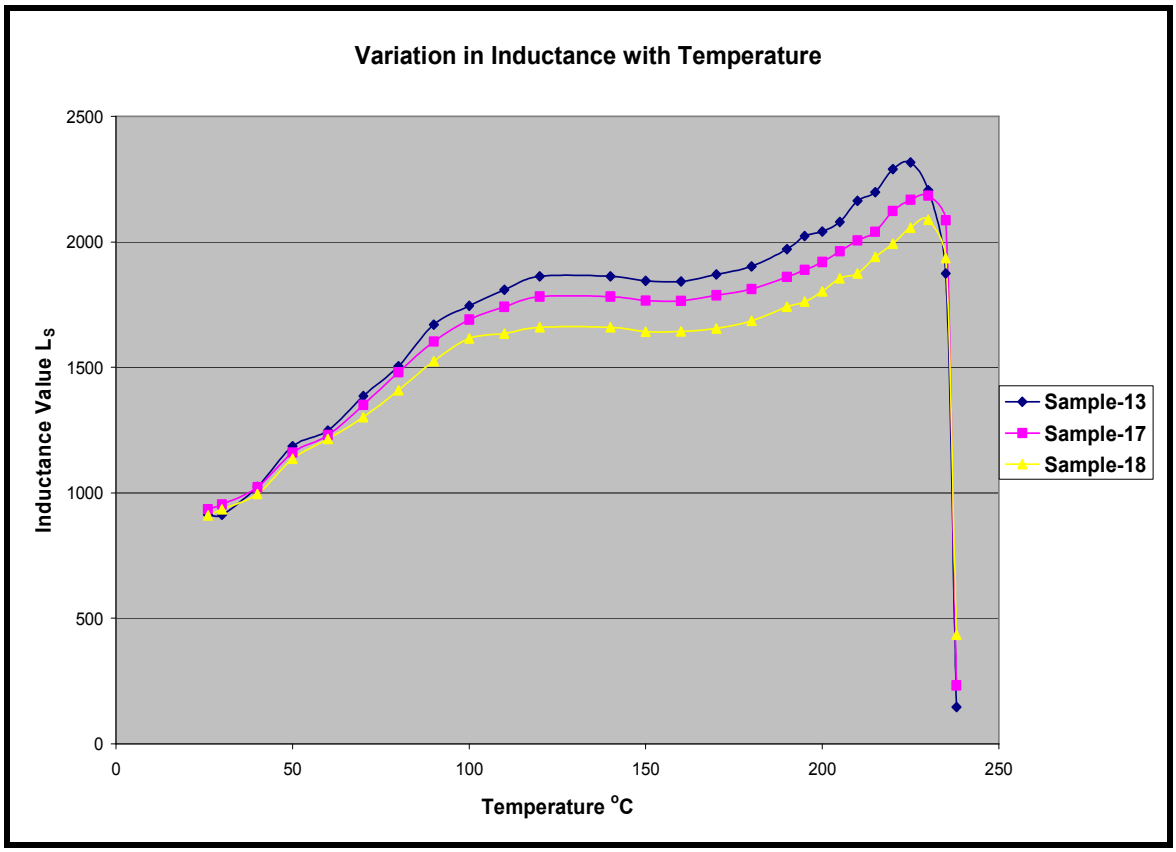

Figure 26- Variation in Inductance with Temperature for selected MnZn ferrite Samples

As revealed by **figure 26** the Inductance value drops drastically after 238 ^{o}C. It is the Curie temperature of the samples at which their magnetic properties are lost, hence we can say these ferrite material can be operated up to 238^{0}C.

4.4 Microstructural Characterization

Microstructures of some selected etched samples at different magnifications are given in the **figure 27.**

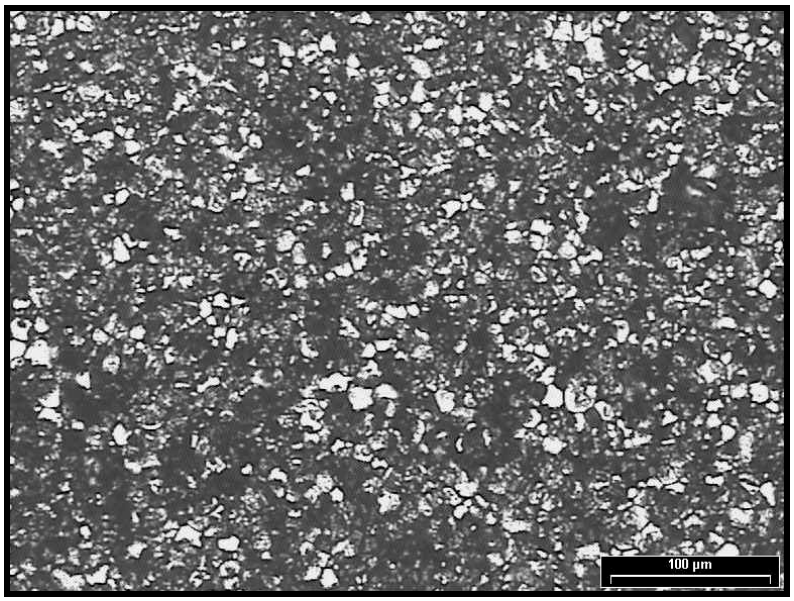

Figures 27(a)-Optical Micrograph of Sample 1 at 100 X.

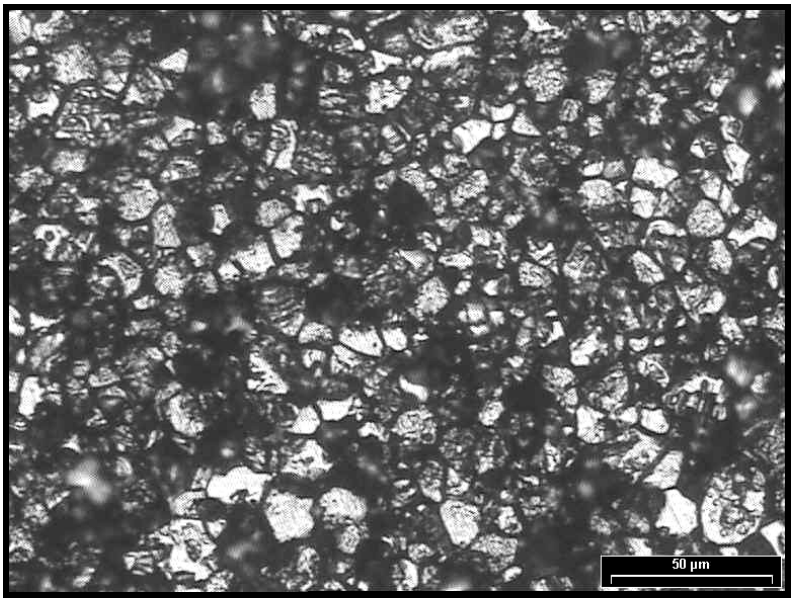

Figures 27(b)-Optical Micrograph of Sample 1 at 200 X.

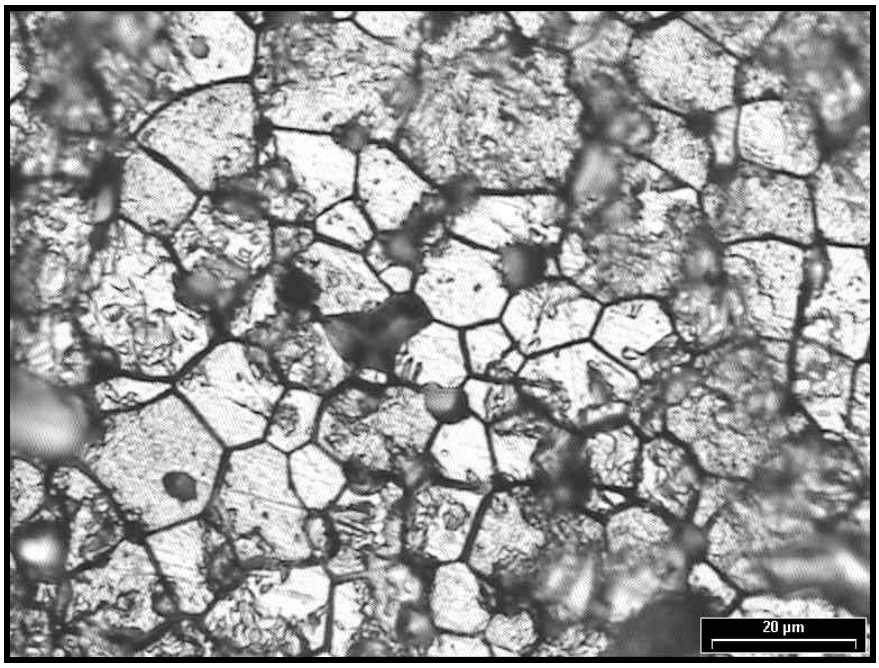

Figure 27(c)-Optical Micrograph of Sample 1 at 400 X.

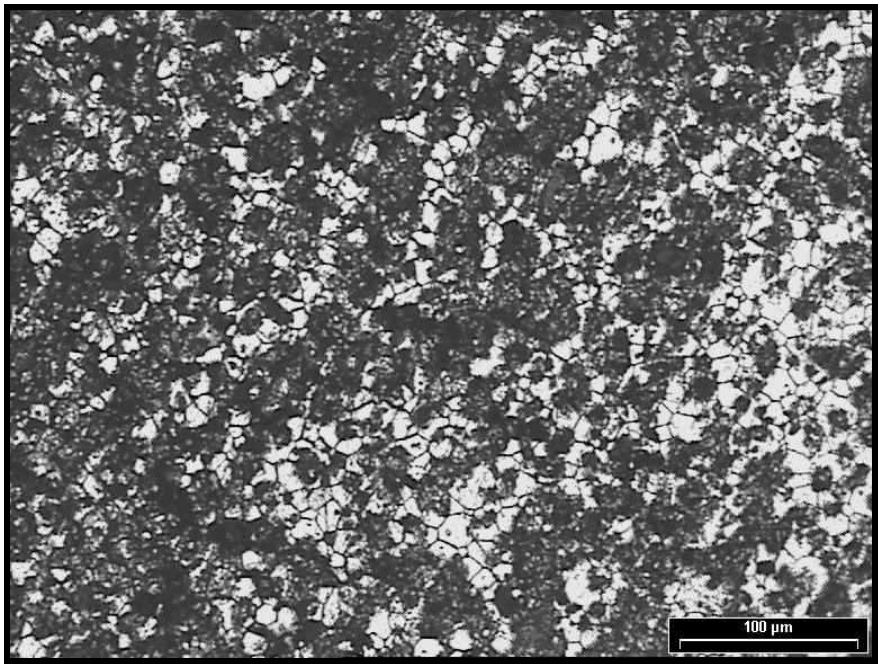

Figures 28(a)-Optical Micrograph of Sample 5 at 100 X.

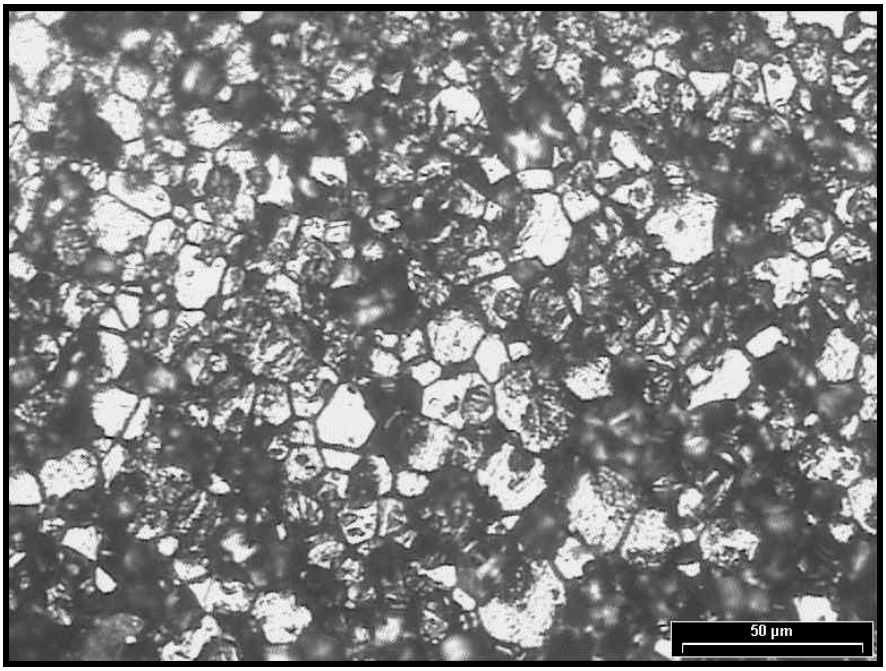

Figures 28(b)-Optical Micrograph of Sample 5 at 200 X.

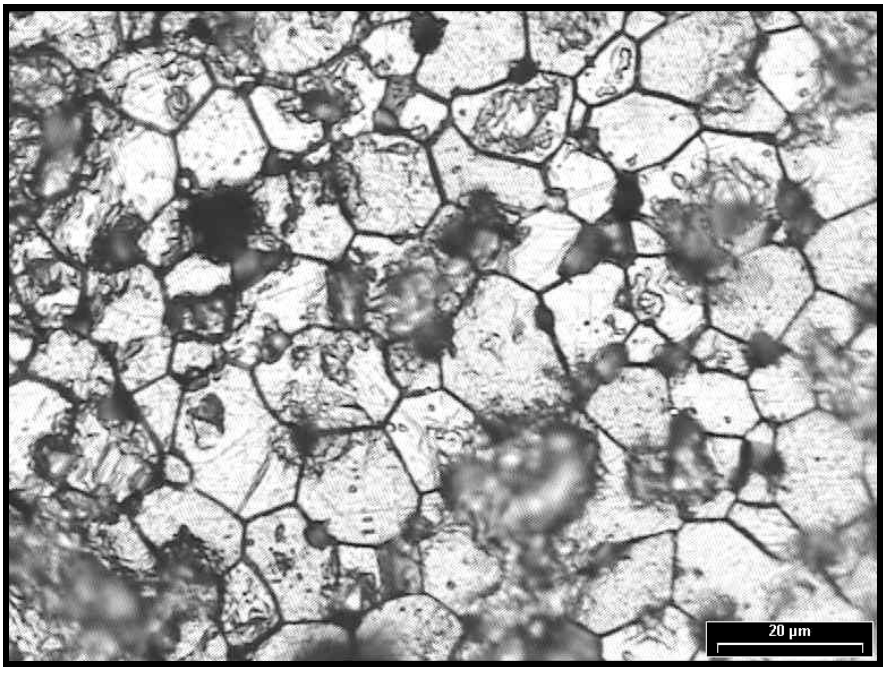

Figures 28(c)-Optical Micrograph of Sample 5 at 400 X.

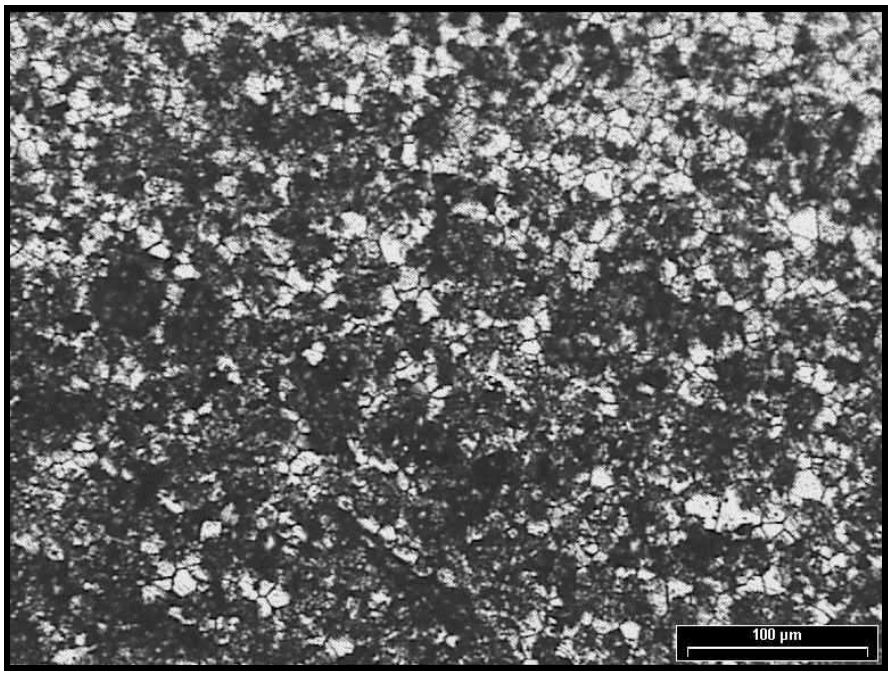

Figures 29(a)-Optical Micrograph of Sample 17 at 100 X.

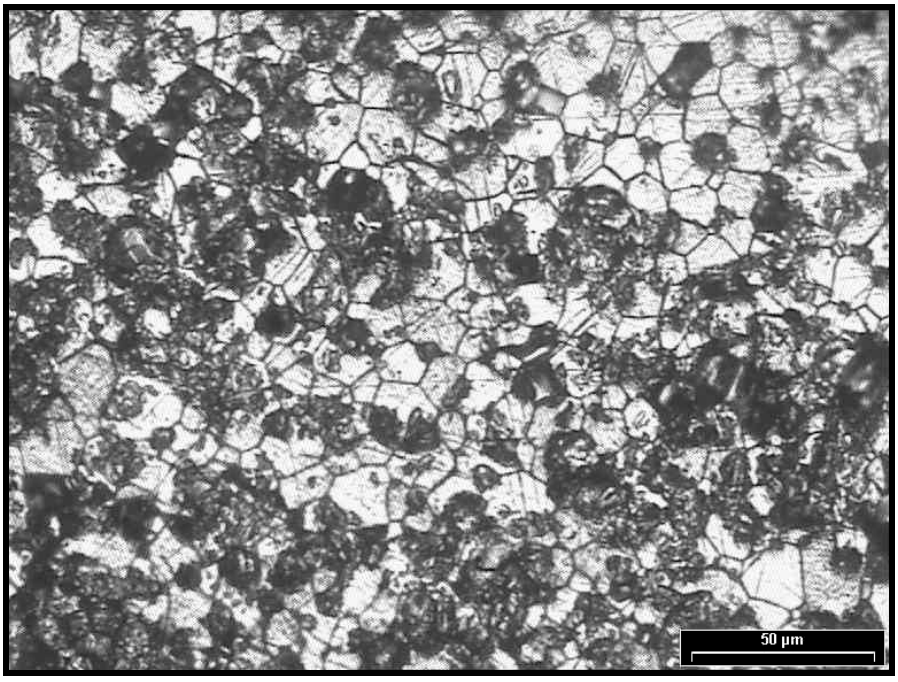

Figures 29(b)-Optical Micrograph of Sample 17 at 200 X.

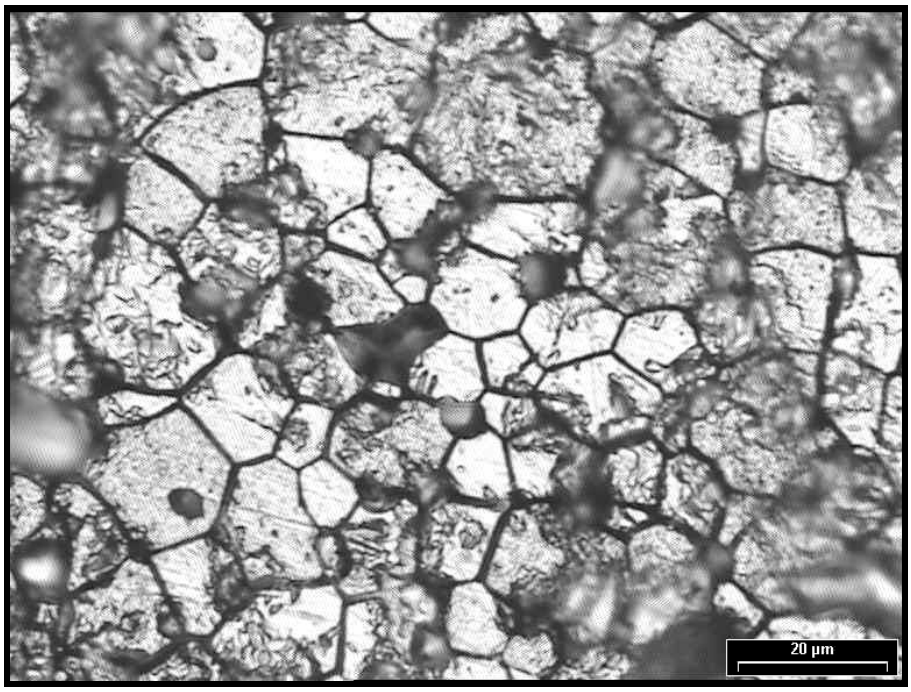

Figures 29(c)-Optical Micrograph of Sample 17 at 400 X.

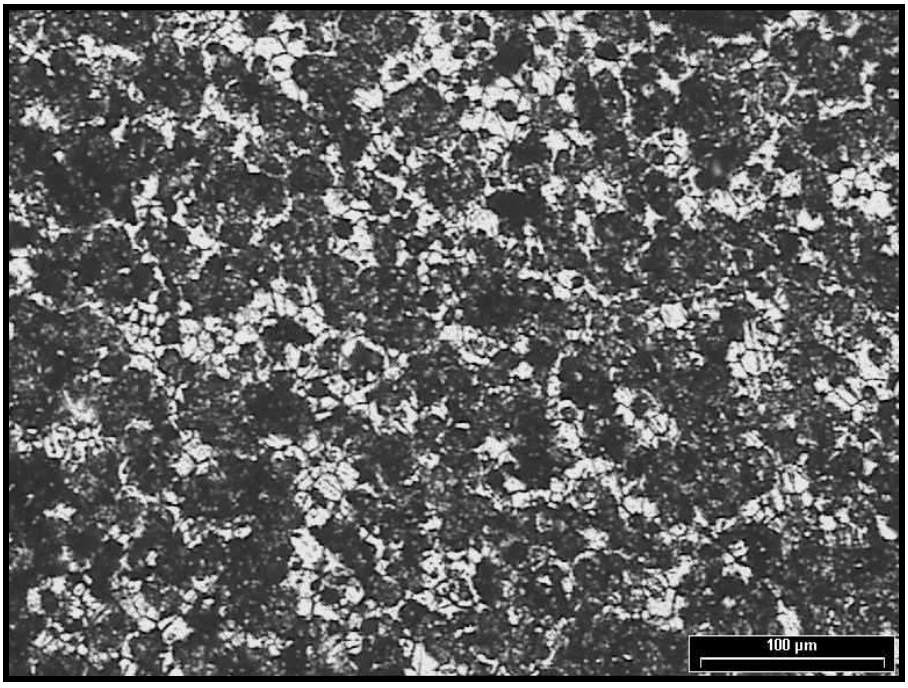

Figures 30(a)-Optical Micrograph of Sample 18 at 100 X.

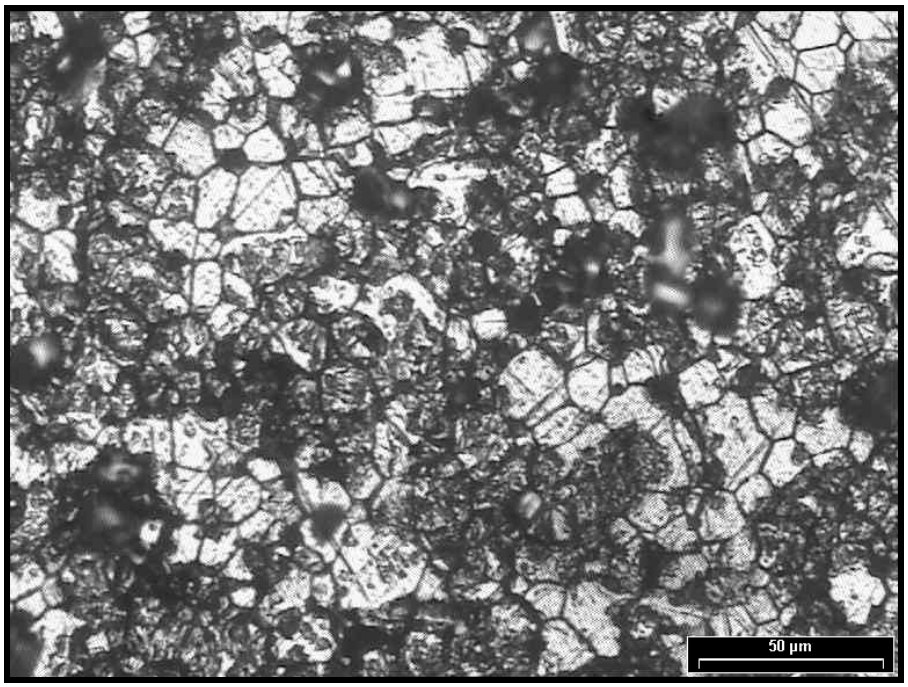

Figures 30(b)-Optical Micrograph of Sample 18 at 200 X.

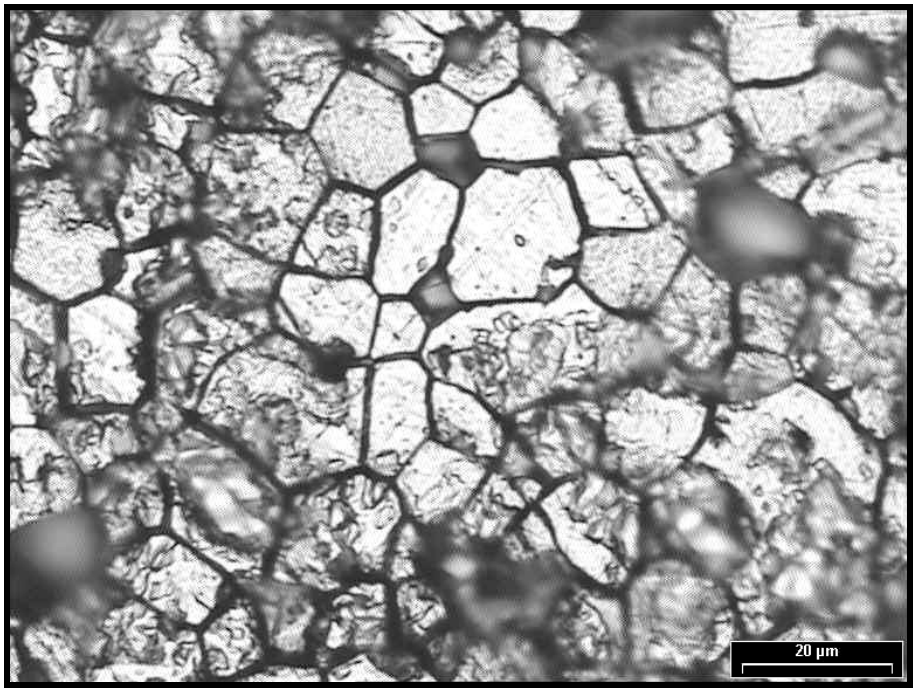

Figures 30(c)-Optical Micrograph of Sample 18 at 400 X.

CHAPTER 5

CONCLUSIONS

The present work reports the serial development of a MnZn ferrite material of basic composition 53.23 mole%, 35.6 mole%, 11.17 mole% and forming the chemical formula $\mathbf{Mn_{0.712}Zn_{0.223}Fe_{2.12}O_{4.12}}$ with traces of some additives, suitable for power applications. X-ray diffraction pattern of the crushed powder of the sintered core reveals the formation of ferrite phase.

The suitable combination of this ferrite composition with 0.05% Calcium oxide, 0.01% Silica, 0.02% Niobium oxide, 0.02% Zirconium oxide and 0.06% Cobalt oxide, processed under strictly controlled sintering profile results in the prospective material for power loss application.

A power loss value of 553 Kw/m^3 and 328 Kw/m^3 could be realized at a frequency of 100 KHz and a driving flux density of 200 mT at 25 and 100^{o}C respectively. The lowest power loss value is reported between 90-110 ^{0}C, as against less than 80^{0}C for conventional MnZn ferrite materials. Also the material is found to be suitable in the frequency of range of 10-1000 KHz and have the curie temperature of approx. 238^{o}C.

Power loss of less than 350 Kw/m^3 in the temperature range of 70 – 130^{0}C makes it the most promising candidate for being applicable in regular switching power supplies, as well as in main transformers in DC-DC converters for electrical vehicles such as hybrid electrical vehicles. This material can be shaped to any core design and can be used in the Inverter transformers for LCD backlight, AC adapters and chargers of notebook type PC's.

CHAPTER 6

SCOPE OF THE FUTURE WORK

With the advent of nanotechnology a tremendous surge in research on miniaturization and high efficiency electronic devices is on rise. These modern devices exclusively need soft magnetic materials as its basic component. Soft ferrite material is extensively used in inductors, transformers, antenna rods, loading coils, deflection yokes, choke coils, recording heads, magnetic amplifiers, electromagnetic interference (EMI), power transformer and splitter applications, which forms a basic requirement in high technology areas. Mn–Zn ferrites adequately suit these demands and are considered to shape the future advanced technology.

It is the need of hour to reduce the power loss at high frequency in order to meet the current demand of the high efficiency and miniaturization of the electronic devices. Besides low power loss characteristics, extreme temperature stability of power loss (< 300 Kw/m^3 at 100 khz/200mT from 25^0C to 120^0C) is required to achieve this aim. MnZn ferrite material with these properties will certainly enhance fuel efficiency, electric-power saving, down sizing and weight saving.

These extremely outstanding characteristics could be realized by

- Accurate estimation of the composition, taking into account magnetic anisotropy and grain boundary resistivity.
- The use of ultra pure and ultra fine raw materials.

- Proper and appropriate selection of additives and their quantity to meet the grain boundary resistivity requirements.
- Strict and precise control of oxygen partial pressure of the sintering atmosphere.
- Preparing high purity ferrite powders by alternate non conventional processing techniques such as wet chemical synthesis, co-precipitation, mechano-chemical synthesis, sol gel synthesis, hydrothermal synthesis etc.

REFERENCES

1. R.F. Louh, T.G. Reynolds III and R.C. Buchanan, Ceramic Materials for Electronics, 3rd edition, edited by R.C. Buchanan, Marcel Dekker Inc. (2004).

2. K. Ohta,; Kobayashi, N. Jpn. J. Appl. Phys. vol. 3, 1964, p. 576–580.

3. H. Tsunekawa, A. Nakata, T. Kamijo, K. Okutani, R. K. Mishra, and G. Thomas, IEEE Trans. Mag. MAG-15(6), 1855 (1979).

4. A. Žnidaršič, M. Limpel, M. Drofenik, "Effect of Dopants on the Magnetic Properties of MnZn Ferrites for High Frequency Power Supplies", IEEE Trans. Mag. 31(1995)2, 950-953.

5. M. Drofenik, A. Žnidaršič and I. Zajc, "Highly Resistive Grain Boundaries in Doped MnZn Ferrites for High Frequency Power Supplies", J. Appl. Phys. 82(1997)1, 333-340.

6. B. D. Cullity, " Introduction to magnetic materials", Addison – Wesley Publishing Company, Reading, Massachusetts, Menlo Park, California, London, Don Mills, Ontario, pp. 184 – 190.

7. Mitsuo Sugimoto, the Past, Present, and Future of Ferrites, J. Am. Ceram. Soc., 82 [2] 269–80 (1999).

8. Stoppels, D., Developments in soft magnetic power ferrites. J. Magn.Magn. Mater., 1996, 160, 323–328.

9. T. Akashi, Trans. Japan. Inst. Metals 2, 171 (1961).

10. H. Tsunekawa, A. Nakata, T. Kamijo, K. Okutani, R. K. Mishra, and G. Thomas, IEEE Trans. Mag. MAG-15(6), 1855 (1979).

11. A. Znidarsic, M. Limpel, G. Drazic, and M. Drofenik, in ‘‘Ferrites:- Proceedings of The Sixth International Conference on Ferrites,Tokyo,’’ ICF6, p. 333, 1992.

12. K. Ishino, S. Satoh, Y. Takahashi, K. Iwasaki, and N. Obata, in ‘‘Ferrites: Proceedings of The Sixth International Conference on Ferrites, Tokyo,’’ ICF6. 1992.

13. Hideaki Inaba, Teruyoshi Abe, Yoko Kitano, and Junichi Shimomura, Journal Of Solid State Chemistry ,121, 117–128 (1996)

14. Jean-Yves Laval, Local Electrical Behavior, Crystallography, and Chemistry of Grain Boundaries in Mn-Zn Ferrites, J. Am. Ceram. Soc., 81 [5] 1133–40 (1998)

15. Andrej Znidarsic and Miha Drofenik, High-Resistivity Grain Boundaries in CaO-Doped MnZn Ferrites for High-Frequency Power Application, J. Am. Ceram. Soc., 82 [2] 359–65 (1999).

16. V.T. Zaspalis, The effect of Nb2O5 dopant on the structural and magnetic properties of MnZn-ferrites, Journal of Magnetism and Magnetic Materials 250 (2002) 98–109.

17. Chen et al. Improvement on magnetic power loss of MnZn-ferrite materials by V2O5 and Nb2O5 co-doping, Journal of the European Ceramic Society 21 (2001) 1931–1935.

18. J. Nie et al. “The effect of nano-SiO2 on the magnetic properties of the low power loss manganese–zinc ferrites”, Journal of Magnetism and Magnetic Materials 265 (2003) 172–175.

19. J. T’opfer, Microstructural effects in low loss power ferrites, Journal of the European Ceramic Society 25 (2005) 3045–3049.

20. A. Verma et al. Journal of Magnetism and Magnetic Materials. (2005).

21. Ammad H. Qureshi, The influence of hafnia and impurities (CaO/SiO2) on the microstructure and magnetic properties of Mn–Zn ferrites, Journal of Crystal Growth 286 (2006) 365–370.

22. Ott et al. Recent developments of Mn–Zn ferrites for high permeability applications, Journal of Magnetism and Magnetic Materials 254–255 (2003) 535–537.

23. Sezai et al. TDK corporation, Tokyo, US patent application no. US2004/0090302.

24. A. Goldman, Handbook of Modern Ferromagnetic Materials, Kluwer Academic Publishers, Dordrecht, (1999), 135.

25 A. J. Pigram & R. Freer, the Effect of Binder Additions on the Green and Sintered Properties of Mn-Zn Ferrite Ceramics, Ceramics International 21 (1995) 33-41.

26 Stanley J. Lukasiewicz, Spray-Drying Ceramic Powders, J Am. Ceram. SOC, 72 141 617-24 (1989).

27. Effect of External Lubricant on Mechanical Properties of Dry-Pressed Green Bodies, Maruti Uppalapati and David J. Green, J. Am. Ceram. Soc., 88 [6] 1397–1402 (2005).

28. M. Zenger M. Bogs, R. Lucke, G. Schulz, Am. Ceram. Soc. Bull. 74 (1995) 77.

APPENDIX

Table A1- Composition, power loss and Magnetic flux density of the MnZn ferrite samples.

Sample No.	CaO	SiO2	ZrO2	Nb2O5	CoO	Pv at 100 Khz/200mT		Bmax at 16 khz/250 A/m	
						25 °C	100 °C	25 °C	100 °C
1	500	NIL	NIL	NIL	NIL	683	403	465	384
2	500	20	NIL	NIL	NIL	653	367	481	401
3	500	50	NIL	NIL	NIL	644	351	469	391
4	500	70	NIL	NIL	NIL	631	338	475	397
5	500	100	NIL	NIL	NIL	624	338	482	401
6	500	120	NIL	NIL	NIL	632	345	478	396
7	500	150	NIL	NIL	NIL	663	383	460	386
8	1000	NIL	NIL	NIL	NIL	663	377	481	398
9	1000	20	NIL	NIL	NIL	640	351	484	402
10	1000	50	NIL	NIL	NIL	663	384	466	390
11	1000	70	NIL	NIL	NIL	644	371	467	388
12	1000	100	NIL	NIL	NIL	702	423	453	373
13	500	100	200	200	NIL	601	328	470	391
14	500	100	200	200	200	582	328	475	394
15	500	100	200	200	400	592	351	469	391
16	500	100	200	200	600	553	328	481	357
17	500	100	200	200	800	556	348	470	392
18	1000	20	200	200	NIL	579	328	475	391

Table A2- Resistance, Inductance Value and Initial Permeability of the prepared samples.

Sample No.	Resistance KΩ	Inductance Factor A_L(nH)	Inductance Value L_s (μH)	Initial Permeability μi
1	7.3	2634	1054	2128
2	9.3	2762	1105	2186
3	13	2651	1060	2131
4	14	2594	1038	2096
5	17	2544	1018	1998
6	21	2532	1013	2033
7	16	2581	1032	1998
8	13	2673	1069	2121
9	7	2670	1068	2106
10	16	2483	993	2001
11	24	2406	962	1932
12	12	2328	931	1822
13	47	2398	959	1901
14	41	2476	990	1949
15	58	2414	966	1903
16	53	2516	1006	1998
17	49	2483	993	2005
18	37	2428	971	1911

Table A3 - Dimensions, volume and Density of the sintered MnZn ferrite torroid samples.

Sample No.	Outer Diameter [D_1]	Inner Diameter [D_2]	Height [h]	Weight [gms]	Volume	Density [gm/cc]
1	24.61	14.73	12.06	17.47	3679.6649	4.75
2	24.97	14.94	12.3	18.26	3865.0706	4.72
3	24.8	14.84	12.11	17.71	3753.2439	4.72
4	24.84	14.95	12.19	18.04	3765.6816	4.79
5	24.88	14.94	12.48	18.39	3877.6792	4.74
6	24.83	14.98	12.32	18.02	3792.3531	4.75
7	24.86	14.74	12.36	18.12	3888.3364	4.66
8	24.83	14.84	12.24	18.21	3807.8406	4.78
9	24.82	14.9	12.42	18.44	3841.6002	4.80
10	24.89	14.88	12.06	17.82	3768.8307	4.73
11	24.93	14.94	12.16	18.04	3802.0249	4.74
12	24.69	14.76	12.42	17.24	3819.3329	4.51
13	24.68	14.84	12.4	17.96	3785.3268	4.74
14	24.83	14.82	12.31	17.99	3835.3498	4.69
15	24.84	14.87	12.36	17.98	3841.3438	4.68
16	24.97	14.94	12.26	18.2	3852.5012	4.72
17	24.96	14.98	12.13	17.92	3795.5006	4.72
18	24.78	14.92	12.52	18.12	3847.1703	4.71

Table A4 -Variation in Inductance value with Temperature for selected samples at 10 khz/0.05 volts.

Temperature	Sample-13	Sample-17	Sample-18
26	912	934	910
30	912	954	934
40	1024	1022	996
50	1185	1160	1135
60	1248	1230	1214
70	1386	1350	1301
80	1504	1481	1409
90	1670	1602	1525
100	1745	1690	1615
110	1809	1741	1635
120	1863	1782	1659
140	1863	1782	1659
150	1845	1766	1642
160	1842	1765	1643
170	1870	1787	1655
180	1903	1812	1686
190	1971	1860	1741
195	2023	1888	1761
200	2041	1920	1803
205	2080	1962	1855
210	2163	2006	1875
215	2198	2040	1940
220	2290	2123	1993
225	2316	2167	2057
230	2206	2184	2088
235	1875	2086	1936
238	146	232	435

Table A5 - Variation in Initial permeability with frequency

Frequency [Khz]	Sample No.-1	Sample No.-2	Sample No.-3	Sample No.-4	Sample No.-5	Sample No.-8	Sample No.-9	Sample No.-10
10	2056	2053	2016	1970	1985	2046	2011	1944
20	2070	2063	2024	1982	1992	2057	2029	1958
40	2058	2055	2016	1976	1985	2049	2023	1950
100	2062	2059	2020	1974	1989	2053	2021	1952
200	2100	2101	2056	2008	2022	2093	2059	1982
400	2280	2283	2227	2163	2177	2274	2232	2129
1000	3090	3549	3457	3406	3441	3452	3613	3575

Frequency	Sample-11	Sample-12	Sample-13	Sample-14	Sample-15	Sample-16	Sample-17	Sample-18
10	1862	1749	1972	2105	1783	2146	2139	1869
20	1869	1755	1984	2116	1789	2158	2141	1898
40	1862	1749	1974	2103	1785	2146	2139	1886
100	1860	1751	1970	2101	1783	2146	2143	1884
200	1891	1778	2010	2144	1810	2185	2190	1914
400	2021	1903	2188	2360	1933	2390	2395	2057
1000	3295	3169	3633	3391	3321	3436	3467	3232